Dynamic intracellular distribution of Vangl2 during cell polarization in zebrafish gastrula

Isabelle Roszko[1], Diane Sepich[1], Jason R. Jessen[2], Anand Chandrasekhar[3], and Lilianna Solnica-Krezel[1*]

[1] Department of Developmental Biology, Washington University School of Medicine in St. Louis, St Louis, MO 63110

[2] Department of Biology, Middle Tennessee State University, Murfreesboro, TN 37130

[3]Division of Biological Sciences and Bond Life Sciences Center, University of Missouri, Columbia, MO 65211

* Corresponding author: solnical@WUSTL.EDU

Summary

During vertebrate gastrulation, convergence and extension movements elongate embryonic tissues anteroposteriorly and narrow them mediolaterally. Planar Cell Polarity (PCP) signaling is essential for mediolateral cell elongation underlying these movements, but how this polarity arises is poorly understood. We analyzed cell elongation, orientation, and migration behaviors of lateral mesodermal cells undergoing convergence and extension movements in wild-type embryos and mutants for the Wnt/PCP core component Trilobite/Vangl2. We demonstrate that Vangl2 function is required at the time when cells transition to a highly elongated and mediolaterally aligned body. We show that *tri/vangl2* mutant cells fail to undergo this transition and to migrate along a straight path and high net speed towards the dorsal midline. Instead, *tri/vangl2* mutant cells exhibit an anterior/animal pole bias in their cell body alignment and movement direction, suggesting that PCP signaling promotes effective dorsal migration in part by suppressing anterior/animalward cell polarity and movement. Endogenous Vangl2 protein accumulates at the plasma membrane of mesenchymal converging cells at the time its function is required for mediolaterally polarized cell behavior. Heterochronic cell transplantations demonstrated that Vangl2 cell membrane accumulation is stage dependent, and regulated by both intrinsic factors and an extracellular signal, which is distinct from PCP signaling or other gastrulation regulators, including BMP and Nodals. Moreover, mosaic expression of fusion proteins revealed enrichment of Vangl2 at the anterior cell edges of highly mediolaterally elongated cells, consistent with the PCP pathway core components' asymmetric distribution in *Drosophila* and vertebrate epithelia.

Introduction

Gastrulation is a fundamental morphogenetic process that entails a variety of evolutionarily conserved cell movement behaviors to generate germ layers and shape them into the animal body plan. Studies in different model organisms demonstrated that convergence and extension (C&E) gastrulation movements are crucial players that narrow the tissues in the mediolateral (ML) direction while extending them along the anteroposterior (AP) embryonic axis (Keller et al., 2000). Studies in chick, mouse, frog and zebrafish embryos revealed that C&E movements are driven by active cell migration and polarized cell intercalations (ML planar and radial cell intercalations) of mediolaterally elongated cells (Keller et al., 2000; Myers et al., 2002b; Yin et al., 2008). Cell-cell and cell-extracellular matrix interactions also play essential roles in this process (Coyle et al., 2008; Dohn et al., 2013). Whereas the cellular signals that guide C&E movements are not fully understood, the non-canonical

Wnt/Planar Cell Polarity (Wnt/PCP) signaling system is a key actor. Originally discovered in *Drosophila melanogaster,* PCP signaling polarizes cells in the plane of epithelia of many tissues including the eye, wing, abdomen, and thorax (Adler, 2002; Das et al., 2002; Lawrence et al., 2004; Shimada et al., 2001; Strutt, 2001; Tomlinson and Struhl, 1999). In vertebrates, Wnt/PCP signaling is known to polarize both epithelial and mesenchymal tissues (Gray et al., 2011) and has been implicated in many cellular processes such as C&E gastrulation movements, polarization of ciliary structures, neurulation, cartilage morphogenesis and stem cells expansion (Borovina et al., 2010; Bradley and Drissi, 2011; Kuss et al., 2014; Le Grand et al., 2009; Mahaffey et al., 2013; Wada and Okamoto, 2009; Wallingford et al., 2000; Zilber et al., 2013). Genetic studies in *Drosophila* led to the identification of several core PCP components, including the four-pass transmembrane protein Strabismus/Van Gogh (Vang), the seven-pass transmembrane proteins Frizzled (Fz) and Flamingo (Fmi) and the cytoplasmic proteins Dishevelled (Dsh/Dvl), Diego (Dgo), and Prickle (Pk) (Adler et al., 1997; Chae et al., 1999; Gubb et al., 1999; Taylor et al., 1998; Theisen et al., 1994; Usui et al., 1999; Vinson and Adler, 1987; Wolff and Rubin, 1998). PCP signaling in *Drosophila* produces, or is a consequence of, an asymmetric distribution of some core components at the apical cell membrane (Amonlirdviman et al., 2005; Axelrod, 2001; Lawrence et al., 2004; Ma et al., 2003). Vang and Pk are enriched on one side (proximal in the wing) and Fz, Dsh, and Dgo on the opposite side (distal in the wing) of the cell along the planar polarity axis of the tissue, with Fmi being observed at both cell edges (Strutt and Strutt, 2008). As a result of intercellular interactions and intracellular feedback loops, the core protein complexes have been shown to concentrate into discrete membrane subdomains or "puncta" (Strutt et al., 2011). A tight regulation of the composition of these complexes on the opposite cell membranes and consequently on adjacent membranes of two neighboring cells is essential for the polarizing signal to be propagated across several cell diameters (Adler et al., 2000). Recent studies also implicate Wg and Wnt4 in providing long-range directional input in the *Drosophila* wing (Wu et al., 2013). Zebrafish embryos carrying mutations in several of the Wnt/PCP pathway core components and in Wnt11/Wnt5 ligands exhibit a characteristic morphogenetic phenotype, with shorter AP and broader ML body axes due to impaired C&E movements (Heisenberg et al., 2000; Kilian et al., 2003; Marlow et al., 1998).

In vertebrate embryos, C&E movements shape all the germ layers and are coordinated with mesendoderm internalization and epiboly movements. Mesodermal precursors upon internalization via a blastopore migrate away from it, and later turn their trajectories towards the nascent embryonic midline (Solnica-Krezel and Sepich, 2012). In the zebrafish gastrula,

internalized mesodermal cells first move anteriorly, towards the animal pole, but at midgastrulation, they alter their movement trajectories from anterior/animal to dorsal, marking the start of C&E (Sepich and Solnica-Krezel, 2005). At these early C&E stages, mesodermal cells undergo dorsal migration as individuals along irregular paths; however, as gastrulation progresses these cells become ML elongated, and migrate dorsally as a group, faster and along straighter trajectories. This change fails to occur in Wnt/PCP signaling mutants, including *trilobite/vangl2* (*tri/vangl2*) (Jessen et al., 2002), and polarized radial and planar ML intercalations are also impaired (Yin et al., 2008).

How Wnt/PCP signaling contributes to ML cell polarization, polarized cell migration and intercalation is incompletely understood. Increasing evidence suggests that this pathway acts as a cellular compass that coordinates polarity and individual cell behaviors with the AP and ML embryonic axes (Gray et al., 2011; Yin et al., 2008). Similar to the asymmetric distribution of the core PCP components in *Drosophila* epithelia, asymmetric localization of core PCP proteins expressed as fluorescent fusion proteins was observed in ML polarized cells during zebrafish gastrulation, with Pk-GFP and Dvl-GFP fusion proteins being enriched at the anterior and posterior cell membranes, respectively (Ciruna et al., 2006; Yin et al., 2008). By contrast, in *Xenopus* Dvl is enriched at the cell edges facing the notochord-somite boundary (Panousopoulou et al., 2013). Yet, C&E movements in *Xenopus* explants are controlled by the PCP core proteins via the Septin cytoskeleton and its ability to regulate cortical actomyosin compartmentalization and the remodeling of cell-cell contacts (Shindo and Wallingford, 2014). Phosphorylated myosin II, reporter of actomyosin-based contraction, was shown to be enriched at the anterior and posterior cell boundaries (Shindo and Wallingford, 2014), consistent with PCP core proteins' enrichment at these boundaries in zebrafish gastrulae. Asymmetric distribution of Vangl2 was observed in epithelia of the developing ear and skin in adult mouse (Devenport and Fuchs, 2008; Montcouquiol et al., 2006). However, intracellular distribution of Vangl2 during gastrulation is not known.

In this study, we have addressed the dynamics of cell polarization by Vangl2 and its subcellular distribution during zebrafish gastrulation. First, we show that lateral mesodermal cells undergo a transition from a round to ML elongated morphology at a specific time during gastrulation and location relative to the dorsal midline. Because tri/*vangl2* mutant cells fail to elongate and exhibit an abnormal anterior/animal pole bias in their cell body alignment and movement direction, we propose that PCP signaling promotes effective dorsal migration in part by suppressing anterior/animalward cell polarity and movement. Second, our analyses of the endogenous Vangl2 distribution revealed its accumulation at the cell membrane preceding

ML cell elongation and effective convergence to the dorsal midline. Third, based on heterochronic transplantation experiments, we propose that this membrane accumulation of Vangl2 at the onset of C&E is regulated by both a cell-intrinsic mechanism and a non cell-autonomous signal, which is distinct from PCP signaling or other known gastrulation regulators. Finally, we show that Vangl2 accumulates more strongly at the anterior cell membranes in highly ML elongated mesodermal and neuroectodermal cells. These results demonstrate that the dynamic Vangl2 intracellular distribution is coordinated with and necessary for the changes in C&E cell behaviors during gastrulation.

RESULTS

Spatiotemporal dynamics of ML elongation of mesodermal cells during C&E

During zebrafish gastrulation, lateral mesodermal cells converging towards the dorsal midline change their morphology and behavior in a location and stage dependent manner. While this transformation depends on Wnt/PCP signaling and *vangl2* function (Jessen et al., 2002), its timing and underlying cellular and molecular mechanisms remain to be determined. Towards this goal, we first analyzed changes in cell shape and alignment at different positions along the dorsoventral (DV)/ML axis of the wild-type (WT) gastrula by performing time-lapse analyses at late gastrulation stages (9-10hpf). We determined cell elongation, as length to width ratio (LWR), in domains at different positions relative to the dorsal midline (expressed as angular degrees from the dorsal midline: 90˚, 55˚, and 20˚, Fig. 1C) (Topczewski et al., 2001). Our analyses at late gastrulation (9hpf) showed a gradual cell elongation, or increase in the LWR, along the ML embryonic axis, with lower LWR ratio values seen at 90˚ from the dorsal midline (n=7 embryos, 310 cells) and higher LWR values closer (20˚) to the dorsal midline (n=5 embryos, 240 cells) (Fig.1A-B", 1D). Additional analyses 55˚ from the dorsal midline demonstrated dynamic cell shape changes during the course of each time lapse: LWR increased over the 60 min time-lapse (n=7 embryos, 341 cells, and n=6 embryos, 295 cells, respectively), suggesting cell shape transformation occurs at this specific location and time during gastrulation (Fig.1D). Analysis of cell shape changes in *tri/vangl2* and maternal zygotic *tri/vangl2* mutant gastrulae (MZ*tri*$^{vu67/vu67}$ mutants produced by genetically mosaic WT females harboring *tri* $^{vu67/vu67}$ germ cells, generated by germline replacement and therefore lacking both maternal and zygotic *tri/vangl2* function (see Materials and Methods)), showed that mutant cells fail to undergo this change. At both positions 55˚ and 20˚ from the dorsal midline, mutant cells exhibited rounder cell shapes even when compared to those

observed at 90˚ from dorsal location in WT (Fig.1D; 90˚- MZ*tri/vangl2:* n=2 embryos, 140 cells; 55˚- *tri/vangl2*: n=3 embryos, 226 cells; 20˚- *tri/vangl2:* n=3 embryos, 193 cells).

Next, we asked when and where, relative to the changes in cell shape, the mesodermal cells align their long axes with the DV/ML gastrula axis. Analyzing the time-lapse data described above, we observed that in WT gastrulae, the alignment of cell bodies along the ML embryonic axis occurred in a gradual manner. Cells located at 90˚ from dorsal exhibited various degrees of ML alignment, whereas in the region located 20˚ from dorsal, almost all WT cells had their long axes aligned +/- 20˚ with the ML embryonic axis (Fig.1E). By contrast, in *tri/vangl2* and MZ*tri/vangl2* mutant gastrulae, cells failed to ML align, consistent with our previous studies ((Jessen et al., 2002); and Fig.1B-B", 1E). Notably, a significant fraction of *tri/vangl2* cells were aligned along the AP axis, and thus perpendicular to the ML cell alignment, the hallmark of C&E cell behavior (Jessen et al., 2002; Keller et al., 2000; Wallingford et al., 2002)

At the onset of gastrulation, internalized lateral mesodermal and endodermal cells initially move anteriorly, and at midgastrulation turn their trajectories towards the dorsal midline (Dumortier et al., 2012; Sepich and Solnica-Krezel, 2005). In order to better understand the relationship between the cell body alignment and this movement behavior, we analyzed the trajectories of WT and *tri/vangl2* mutant cells. We analyzed cell trajectories in 9.5hpf embryos for 60 minutes (one minute time-point intervals) at 55˚ from the dorsal midline, where the transition in the cell shape occurs (Fig.1D). Because cell behavior and trajectories vary along the AP axis (Sepich et al., 2005), we performed this analysis at different locations along the AP axis: animal, equatorial, and vegetal (anterior to, at the level of, or posterior to the first somite, respectively) (Fig.2B). We observed, as expected, a predominance of cell movements in the dorsal direction (+/-45˚ from the ML axis) in both WT and *tri/vangl2* mutant gastrulae (Fig.2C). In WT, dorsal movement was the most predominant in the equatorial domain compared to the animal or vegetal domains. However, in the *tri/vangl2* mutant gastrulae the proportion of anteriorly/animally directed movements was increased at all locations along the AP axis compared to WT embryos, with the greater increase in the vegetal domain. Moreover, the frequency of vegetally/posteriorly and ventrally oriented movements was decreased in *tri/vangl2* compared to WT gastrulae (Fig.2C). Next, we analyzed cell trajectories according to their "next cell movement direction", defined as the direction (dorsal, animal, vegetal or ventral) the cell adopts compared to its previous movement direction (Fig.2A, (Sepich et al., 2005). We pooled the cell movements according to their initial direction (animal, dorsal, vegetal, ventral) and

determined the direction of the next movement. In WT, the next cell movement was predominantly dorsal at all locations along the AP axis. Notably, in *tri/vangl2* mutants, the fraction of cells moving animally/anteriorly was increased at all AP locations. (Fig.2D). Therefore, unlike WT, *tri/vangl2* mutant cells did not elongate nor align in the ML embryonic axis, and they displayed a slightly animally/anteriorly biased body alignment and movement preference.

Vangl2 accumulates at the plasma membrane at a specific time during gastrulation

Given that the dynamic changes in cell shape and orientation during C&E depend on *tri/vangl2* function ((Jessen and Solnica-Krezel, 2004; Jessen et al., 2002); Fig.1), we wanted to determine the subcellular distribution of Vangl2 protein during this process. We generated a polyclonal antibody against the cytosolic C-terminal domain of Vangl2 ((Li et al., 2013), Fig.3). Whole mount immunofluorescence experiments revealed that Vang2 was present at high levels at the membrane of mesodermal and ectodermal cells during late gastrulation beginning at 8hpf (Fig.3C-D, F). By contrast, at blastula (3 and 4hpf) and early gastrula (6hpf) stages the protein was preferentially detected in cytoplasmic puncta (Fig.3A, Fig.S2, Fig.S3). Low levels of Vangl2 protein were occasionally observed at cell membranes at and before shield stage (6hpf) (Fig.S3A-G). These data demonstrate that Vangl2 localization is dynamic during gastrulation and it accumulates at the cell membrane at the stages when tri/*vangl2* function is required for proper C&E cell behaviors.

Vangl2 membrane accumulation is independent of signaling pathways that pattern vertebrate gastrulae

We next wished to understand the mechanism underlying the membrane accumulation of Vangl2 at the onset of C&E movements. Gastrulation movements are both spatially and temporally coordinated with embryonic axis formation and patterning (Myers et al., 2002a). Morphogen gradients, including BMP or Nodal, are known to regulate expression of some PCP genes during gastrulation (e.g. *wnt11, wnt5*) (Gritsman et al., 1999; Myers et al., 2002a). To test whether Vangl2 membrane accumulation is dependent on Nodal signaling we performed whole mount immunostaining on MZ *one-eyed pinhead*^{tz257tz257} *(*MZ*oep)* mutant gastrulae, where the essential Nodal cofactor, EGF-CFC/Cripto is inactive (Gritsman et al., 1999). We found that Vangl2 was localized to cell membranes in MZ*oep* mutants at early segmentation stages indicating Nodal signaling is not necessary for Vangl2 membrane localization (Fig.4A-A'). Next we asked whether Vangl2 distribution was regulated by the

ventral to dorsal BMP activity gradient that limits C&E movements to the dorsolateral gastrula regions (Myers et al., 2002a). We observed that, at early segmentation stages, Vangl2 was localized at cell membranes in MZ*ichabod* mutant embryos (Fig.4B-B'), which have very reduced level of *β-catenin2,* fail to form Spemann-Mangold gastrula organizer and consequently show strong upregulation of BMP signaling and severe ventralization (Kelly, Chin et al. 2000). Finally, downregulation of BMP signaling by injecting synthetic mRNA encoding the BMP antagonist Noggin, resulted in severe embryo dorsalization, but did not affect Vangl2 membrane localization (Fig.4C-C')(Bauer et al., 1998; Furthauer et al., 1999; Hammerschmidt et al., 1996). Together, these data indicate that the two key morphogens involved in embryo patterning, BMP and Nodal, are not essential for Vangl2 membrane accumulation during gastrulation.

To test further the possible relationship between the ventral to dorsal gastrula patterning and Vangl2 we performed whole mount immunostaining using anti-Vangl2 antibody at midgastrulation (8.4hpf) and quantified membrane fluorescence intensity in ventral, lateral, and dorsal gastrula domains. We did not observe significant differences in the accumulation of Vangl2 at cell membrane between these domains (Fig.S4). This observation provides further support against the ventrodorsal gradient of BMP or another regional signal regulating Vangl2 membrane accumulation during gastrulation.

We next tested whether Vangl2 membrane accumulation requires Wnt/PCP signaling. We observed that in 10.7hpf WT embryos mosaically expressing Xdd1, a dominant negative mutant form of *Xenopus* Dsh that impairs noncanonical Wnt signaling and C&E movements in frog and zebrafish (Jessen et al., 2002; Sokol, 1996; Wallingford et al., 2000), groups of cells expressing *Xdd1* did not present any perturbation in Vangl2 membrane localization compared to the neighboring cells (Fig.5A-A'). Likewise, we observed normal Vangl2 membrane localization at 10.7hpf in *kny/gpc4*$^{fr6/fr6}$, *MZlandlocked/scribble1*$^{rw468/rw468}$, and MZ*fz7a*$^{e3/e3}$;*MZfz7b*$^{hu3465/hu3465}$ mutants (Fig.5), all defective in PCP signaling (Quesada-Hernandez et al., 2010; Topczewski et al., 2001; Wada et al., 2005). Vangl2 was also detected at cell membranes of WT cells transplanted into *MZtri*$^{vu67/vu67}$ mutants, suggesting that Vangl2 membrane localization is independent of its presence at the cell membrane in the adjacent cell (Fig.5E). These results indicate that key signaling pathways that pattern vertebrate gastrulae and/or regulate C&E movements, including BMP and Nodal, and Wnt/PCP signaling are not necessary for Vangl2 localization to the plasma membrane.

Vangl2 membrane accumulation at midgastrulation is regulated both cell-autonomously and by a stage-specific non-autonomous global signal

To understand whether Vangl2 membrane accumulation at the onset of C&E is a cell-autonomous process or is mediated by a non cell-autonomous signal, we performed heterochronic transplantation experiments between WT embryos of different developmental stages (Fig.6A). In the first set of experiments, cells were transplanted from sphere stage (4hpf) donors into germ ring/shield stage (5.5-6hpf) hosts. When donor embryos reached the shield stage and host embryos the 75-80% epiboly stage (8-8.4hpf), Vangl2 protein localization was assessed by whole mount immunostaining and its membrane localization was quantified in confocal microscopic images (Fig.6B-C",G). The intensity of Vangl2 expression on cell membranes was normalized to background (interior of the same cell). Homochronic transplantations with sphere stage donors and hosts were carried out as control, and analyzed by Vangl2 staining at 8hpf (Fig.6F). These experiments indicated that, unlike in homochronic transplantations, the cells transplanted from "younger" donors into "older" host embryos showed significantly higher amounts of Vangl2 protein at cell membrane compared to that observed in the younger donor embryo from which they were removed (Fig.6G). However, Vangl2 membrane localization levels in these "younger" donor cells did not reach the level observed in the surrounding "older" host cells. These results suggest that Vangl2 membrane localization is stimulated in the "younger" donor cells by a non cell-autonomous signal when transplanted into an "older" WT host embryo, but that a cell-intrinsic mechanism is also involved. To test this further, we performed a reverse heterochronic transplantation experiment by moving cells from an older (shield stage; 6hpf) donor into a younger (sphere stage; 4hpf) host embryo. Vangl2 membrane localization was assessed as described above, when the younger hosts reached shield stage and donor embryos the 75%-80% epiboly stage (8-8.4hpf) (Fig.6D-E"). In these experiments the level of Vangl2 membrane localization in the cells transplanted from "older" donors was lower than in the cells of the donor embryo, but higher than in cells of the younger host embryo (Fig.6H). These results further support an involvement of a cell-autonomous mechanism of Vangl2 membrane accumulation at a specific stage of gastrulation. However, considering that Vangl2 protein levels at the membrane were lower in transplanted "older" cells than in the original donor embryos, non-autonomous global signals also regulate Vangl2 accumulation at the cell membrane at midgastrulation, when increasing C&E movements take place (Sepich et al., 2000).

Vangl2 localizes asymmetrically in highly polarized gastrula cells

While polarized intracellular distribution of Vangl2 has been observed in the developing ear and skin epithelia in the mouse (Devenport and Fuchs, 2008; Montcouquiol et al., 2006), whether this core Wnt/PCP component shows asymmetric localization during vertebrate gastrulation remains to be determined. Given the previously reported asymmetric localization of PCP components Pk and Dvl in vertebrate gastrulae at the anterior and posterior cell membranes, respectively, we hypothesized that Vangl2 is enriched at the anterior cell membrane, where Pk is enriched (Ciruna et al., 2006; Yin et al., 2008). To test this we used several approaches to quantify the amount of Vangl2 protein at the anterior and posterior cell membranes. First, we performed whole mount immunofluorescence on WT embryos with anti-Vangl2 antibody, acquired confocal images and measured the fluorescence intensity at the cell membranes. This quantification based on the merged anterior/posterior and medial/lateral cell boundaries showed no obvious asymmetric pattern of Vang2 protein distribution in the presomitic mesoderm (data not shown).

Second, we adopted the mosaic approach that allows visualizing protein distribution asymmetries on single anterior or posterior membranes using a transgenic line expressing zebrafish GFP-Vangl2 N-terminal fusion protein (Sittaramane et al., 2013). We transplanted a few cells from *Tg(vangl2:GFP-Vangl2)* embryos injected with *mCherry* synthetic mRNA (used as a control) into unlabeled WT host embryos. Confocal images were acquired at the dorsal location at 90% epiboly stage (9hpf) when C&E movements are the most dramatic, and at 5-6s stage (11.7-12hpf) when cells are extremely polarized. We quantified the FI at the anterior and posterior cell membrane of isolated cells for both GFP-Vangl2 and mCherry proteins using the plot profile tool (Fiji) and calculated the ratio Posterior/Anterior membrane FI of GFP-Vangl2 and mCherry for each cell. At 9hpf in the notochord, GFP-Vangl2, like mCherry did not show any significant difference between the FI at the anterior and posterior cell membranes (n=23 cells, 4 embryos) (Fig.7A-A',D). However, at segmentation stages (11.7-12hpf), in the notochord (n=23 cells, 8 embryos) and neuroectoderm (n=15 cells, 4 embryos) we observed an anterior bias in GFP-Vangl2 localization; contrasting random anterior or posterior enrichment observed for mCherry protein (Fig.7B-C',E). As an alternative approach, we used mosaic expression of the human GFP-VANGL2 N-terminal fusion protein (construct provided by the Ogura lab, Tohoku University, Japan). Indicating that the GFP-VANGL2 protein has normal activity, after injection of synthetic *GFP-VANGL2* mRNA (25pg–75pg/embryo) we observed partial but significant rescue of the axis elongation phenotype in the MZ*tri*$^{vu67/vu67}$ (Fig.S1), comparable with previously reported incomplete

rescue of the *tri* mutant phenotype using synthetic WT zebrafish *vangl2* mRNA (Jessen et al., 2002). In addition, we observed that similarly to the endogenous protein, GFP-VANGL2 became localized at the cell membranes at late gastrulation and segmentation stages (Fig.7G). These results indicate that the activity of GFP-VANGL2 fusion protein during gastrulation is comparable to that of the zebrafish Vangl2 protein. To express GFP-VANGL2 in a mosaic fashion, we injected synthetic *GFP-VANGL2* mRNA into one blastomere of WT embryos at 64-cell stage (Fig.7F), after first titrating the *m*RNA to find the concentration enabling us to visualize fluorescence without causing gastrulation defects due to excess *VANGL2* expression (Jessen et al., 2002). *mCherry* mRNA was co-injected as a control. Confocal images were acquired during early segmentation and we focused on highly polarized notochord cells. The FI of GFP-*VANGL2* and mCherry was quantified as above. Compared to mCherry, which exhibited random anterior/posterior enrichment, GFP-VANGL2 levels were consistently higher at anterior cell membranes (Fig.7H,I) (n=12 cells, 3 embryos). Together these lines of experimentation support the notion that Vangl2 is asymmetrically localized in highly polarized notochord and neuroectoderm cells at early segmentation stages, but not in less polarized cells during gastrulation.

We next asked whether the anterior bias in Vangl2 membrane localization is dependent on functional Wnt/PCP signaling. We either injected a minimal dose of *GFP-VANG2* into one cell of a 64-cell stage *MZfz7a*$^{e3/e3}$*; MZfz7b*$^{hu3465/hu3465}$ and *kny*$^{fr6/fr6}$ mutant embryos or, we transplanted few cells from *Tg(vangl2:GFP-Vangl2)* embryos co-injected with *Xdd1* and *mCherry* mRNA and into WT host previously injected with the same dose of *Xdd1* mRNA. We quantified the membrane FI exclusively in individual cells present in the notochord, at 5-6s stage (11.7-12hpf) as described above. Our data showed that perturbation of PCP pathway in *MZfz7a*$^{e3/e3}$*; MZfz7b*$^{hu3465/hu3465}$ (n=27 cells, 7 embryos) and *Xdd1* injected embryos (n=27 cells, 8 embryos) did not result in a significant loss of the anterior bias in Vangl2 localization (Fig.8A-A',C). By contrast, *kny/gpc4*$^{fr6/fr6}$ mutants showed significantly decreased Vangl2 polarization, although not a total loss of polarity (n=43 cells, 7 embryos) (Fig.8B-C).

Given that Vangl2 showed reduced anterior bias at the membrane when the PCP is perturbed, next we wished to ask if this bias is cell autonomous. To this goal, we transplanted cells expressing GFP-Vangl2 from *Tg(vangl2:GFP-Vangl2)* embryos injected with *mCherry* mRNA into unlabeled *MZtri*$^{vu67/vu67}$ host embryos. We selected and imaged embryos that contained individual GFP-Vangl2/mCherry expressing cells surrounded by *MZtri*$^{vu67/vu67}$ host cells in the notochord. Quantification of the FI at the anterior and posterior membranes of

these cells revealed that GFP-Vangl2 was not asymmetrically localized, and presented a random membrane preference similar to the one observed for mCherry (n=27 cells, 7 embryos) (Fig.8C). This result revealed a non-autonomous Vangl2 function for its preferential anterior membrane localization.

DISCUSSION

During C&E gastrulation movements in zebrafish, dorsally migrating mesodermal cells undergo a remarkable transformation from round cells migrating along complex trajectories to mediolaterally elongated cells that move efficiently along straighter paths in a Wnt/PCP dependent manner (Sepich et al., 2005; Sepich and Solnica-Krezel, 2005). The Wnt/PCP pathway has been proposed to act as a cellular compass that links the embryonic AP or tissue proximo-distal polarity to that of individual cells, with some pathway components accumulating at the anterior and others at the posterior (or proximal and distal) cell membranes (Adler, 2002; Adler et al., 2000; Amonlirdviman et al., 2005; Bastock et al., 2003; Devenport and Fuchs, 2008; Gao et al., 2011; Gray et al., 2011). However, the sequence of these morphologic transformations and how are they affected by Wnt/PCP signaling was not clear. In this study we delineate the sequence of the morphologic transformations that the dorsally converging mesodermal cells undergo, identify the role of Tri/Vangl2 core PCP component in these transformations, and the accompanying dynamic changes in intracellular distribution of Vangl2 protein. We show that Vangl2 membrane accumulation preceding ML cell polarization relies on both cell-intrinsic and non cell-autonomous mechanisms. Moreover, Vangl2 localizes preferentially at the anterior cell membrane in ML polarized notochord and neuroepithelial cells.

Using time-lapse analyses we visualized the entire morphologic transformation from round to ML elongated mesodermal cells engaged in dorsal convergence. Our analysis of cell shape in different domains (90˚, 55˚ and 20˚ from dorsal) along the ML axis is consistent with previous studies indicating that cells present a more elongated cell shape when closer to the dorsal midline (Myers et al., 2002a; Shih and Keller, 1992). Interestingly, we show that cells in a single location gradually increase their LWR over time. Concomitant with cell body elongation, ML cell alignment occurs gradually between the three ML domains and, also in time, in the same domain (Fig.1E). The process of cell elongation and ML alignment could be regulated by cell-intrinsic mechanism or by stage specific secreted signal(s) or both. We previously demonstrated that Vangl2 has both cell-autonomous and non-autonomous function

in ML cell elongation (Jessen et al., 2002). Rho kinase 2 (Rok2) and $G\alpha_{12/13}$, both regulators of the actin cytoskeleton, have been shown to regulate cell polarity and cell behavior during gastrulation, with $G\alpha_{12/13}$ acting in cell-autonomous manner and likely in parallel to Wnt/PCP (Lin et al., 2005), and Rok2 affecting cell shape cell-autonomously but ML cell alignment in a non cell-autonomous manner acting downstream of Wnt/PCP (Lin et al., 2005; Marlow et al., 2002). Although a link between cytoskeleton and Wnt/PCP has been established, stage/domain specific signals instructing such cytoskeletal regulators remain to be clarified. Our study demonstrates that Vangl2 is essential for cells to undergo location and time specific cell elongation and alignment. As Rok2 has been proposed to act downstream of Wnt/PCP signaling, it will be important to understand the activity of this kinase in the morphological transformation of mesodermal cells during C&E described here.

Our analyses revealed that *tri/vangl2* mesodermal cells present an abnormal AP bias of cell alignment and trajectories (Fig.1,2). Previous cell behavioral analyses showed that at the onset of gastrulation the trajectories of lateral mesodermal cells are oriented animally/anteriorly, but these trajectories become dorsally biased at midgastrulation (Jessen et al., 2002; Sepich et al., 2005). It has been hypothesized that a repulsive signal from the blastopore/blastoderm margin or an attractive signal from the animal pole guide the early animal/anterior migration of mesodermal cells away from the blastopore. The signals underlying the 90-degree shift in movement direction are unknown, but Wnt/PCP signaling is not absolutely required for dorsalward movement (Sepich and Solnica-Krezel, 2005; Yin et al., 2008). Rather, a dorsal midline-derived chemokine has been hypothesized to explain the dorsal migration based on computational modeling (Sepich and Solnica-Krezel, 2005). Moreover, epiboly movements that occur simultaneously with C&E and which are posteriorly/vegetally directed, have another potential influence on cellular trajectories (Sepich and Solnica-Krezel, 2005; Warga and Kimmel, 1990). In our analysis at late gastrulation to 1s stage, WT cells located 55˚ from dorsal domain exhibited a significant dorsal movement preference (Fig.2). *tri/vangl2* cells also migrated dorsally, however, their trajectories were slightly animally/anteriorly biased in all analyzed domains along the animal-vegetal/AP axis (Fig.2D). This anterior bias in *tri/vangl2* mutant cells' movement could be due to their persistent perception of the discussed above attractive or repulsive signal along the AP axis that guides the animal migration of lateral mesodermal cells at early gastrulation (Sepich and Solnica-Krezel, 2005). It is intriguing that Vangl2 and PCP signaling may promote effective dorsal migration in part by suppressing the anterior/animalward cell polarity and movement. The nature of the signal guiding mesodermal migration away from the blastoderm margin is

not known in zebrafish, but FGF8 was proposed to have this activity in the chick gastrula (Yang et al., 2002).

We detected Vangl2 protein, using an antibody specific to the zebrafish protein (Li et al., 2013), largely in cytoplasmic puncta at early gastrulation, but predominantly at the plasma membrane at mid-gastrulation, just preceding initiation of PCP-dependent ML cell elongation (Fig3, FigS2, FigS3). Given that Vangl2 protein is a four-pass transmembrane protein, the punctate pattern observed at early gastrulation could be due to the accumulation of Vangl2 protein in vesicular cargos and endoplasmic reticulum. In murine neural tissues, Vangl2 is selectively sorted into COPII vesicles by Sec24b for the transport from the endoplasmic reticulum to the Golgi (Merte et al., 2010). Interestingly, Rack1 has been identified as a protein interacting with Vangl2 and shown to regulate C&E during gastrulation, oriented cell division, and cellular polarization. Injection of *rack1*-MO prevented membrane localization of EGFP-Vangl2 fusion protein expressed in zebrafish embryos (Li et al., 2011). However, it is still unclear what signal(s) triggers this interaction and it would be interesting to test weather *rack1* depletion affects localization of endogenous Vangl2.

We addressed the mechanism of Vangl2 membrane accumulation by heterochronic transplantations. The amount of Vangl2 protein at the cell membranes in the cells transplanted from older to younger embryos was decreased compared to cells of the donor embryo, but it was higher in these cells compared to the cells in the younger host embryo (Fig6). In the reverse experiment, where groups of younger cells were transplanted into older host, the amounts of Vangl2 protein at the membrane were higher in the transplanted cells, compared to the younger donor embryo, however they did not match the levels observed in the older hosts. Together, these results support the notion that the accumulation of Vangl2 protein at the plasma membrane during gastrulation depends both on cell intrinsic as well as cell non-autonomous mechanisms. Whereas, the extracellular cue(s) and cell-autonomous mechanism involved remain to be defined, we showed that neither of the global patterning regulators Nodal or BMP is required for Vangl2 localization to the cell membrane. Furthermore, Vangl2 accumulates at the membrane independent of the location along the dorsoventral gastrula axis, implying that ventral-dorsal patterning does not regulate Vangl2 membrane accumulation. Finally, our experiments argue against the involvement of the PCP components Knypek/Gpc4, Frizzled7a and Fz7b, Dvl, or Scribble1 in this process. However, other global signaling pathways could be involved in this process. For instance in this study, we did not address the involvement of the FGF (Fibroblast Growth Factor) pathway, which

has been implicated in C&E movements in the chick and frog embryos (Nutt et al., 2001; Yang et al., 2002). It is intriguing that post-translational modifications could regulate Vangl2 intracellular localization during gastrulation. Indeed, Vangl2 has been shown to be subject to phosphorylation in its N-terminal domain under the control of Wnt5a in mouse limb development (Gao et al., 2011). Vangl2 phosphorylation is required for and modulates its activity. In zebrafish, phosphorylation of Vangl2 is a possibility that warrants further investigation.

Similarly to *Drosophila,* where some core PCP components assume asymmetric distribution at the apical cell junctions (Amonlirdviman et al., 2005; Axelrod, 2001; Lawrence et al., 2004; Ma et al., 2003), studies in zebrafish using GFP fusion proteins have shown that in the dorsal mesoderm and neuroectoderm, Pk-GFP and Dvl-GFP are asymmetrically localized at the anterior and posterior cell membranes respectively (Ciruna et al., 2006; Yin et al., 2008). In the mouse limb mesenchyme, functional Wnt/PCP is essential for the asymmetric distribution of Vangl2 and proximo-distal polarization of chondrocytes (Gao et al., 2011). In the present study, using different approaches to quantify mosaically expressed GFP-Vangl2 protein at the cell membranes, we observed that Vangl2 protein at all cell membranes of mesenchymal cells during gastrulation, but preferentially enriched at the anterior membrane of dorsal mesodermal and neuroectodermal cells. However, our methods did not allow us to detect Vangl2 protein asymmetry in less polarized cells undergoing C&E, including notochord (late gastrulation, 9hpf). This result is consistent with previous data showing that Pk asymmetric membrane localization is detectable at 10hpf and not at midgastrulation (8hpf) (Yin et al., 2008). In contrast to the *Drosophila* system, where in epithelial tissues the asymmetry of core PCP components was shown to be very pronounced, in zebrafish gastrulae these asymmetries are less clear likely due to the dynamic nature of mesenchymal cells during gastrulation. In *Drosophila*, the asymmetric accumulation of the core PCP components at opposite cell membranes is a gradual process and is preceded by their accumulation at the membrane in uniform fashion (Strutt, 2002). This mechanism might be similar in vertebrates where asymmetric Wnt/PCP proteins distribution arise gradually and being detectable only in highly polarized cells. Furthermore, Vangl2 asymmetry at cell membranes in the axial mesoderm was not affected in *fz7a,fz7b* mutants or embryos expressing Xdd1, and it was significantly reduced, but not abolished in *kny* mutants. These observations are consistent with the Pk-GFP and Dvl-GFP asymmetries being reduced in *kny* and *tri* single mutants and almost completely absent in *kny;tri* compound mutants (Yin et al., 2008). We interpret these results to mean that the PCP components' asymmetric distribution

requires PCP signaling, but even low levels of PCP signaling are sufficient. Intrestingly, Vangl2 polarity was lost in WT cells transplanted into MZ*tri*$^{vu67/vu67}$ mutant gastrulae, suggesting that Vangl2 asymmetric localization is cell non-autonomous (Fig.8C). Since Vangl2 asymmetric localization was not lost in embryos with reduced Wnt/PCP signaling and cell polarity, but was lost in a Vangl2 null background, we hypothesize that it requires PCP signaling and/or interaction of protein complexes necessary containing Vangl2 and possibly Flamingo/Celsr on opposite membranes of neighboring cells (Strutt and Strutt, 2008). Future studies will explore the molecular mechanisms underlying the emergence of the core PCP proteins' intracellular asymmetries and how they effect the associated changes in cellular morphology and behavior during C&E movements.

Materials and methods

Zebrafish lines and husbandry

Wild-type zebrafish (AB*, Tübingen and hybrids) and fish carrying mutations in *trilobite* (*tri*^{vu67}*)/vangl2, fz7a*^{e3}*;fz7* ^{hu3495}*, knypek*^{fr6} (Topczewski et al., 2001), *scribble1b* (originally described as *landlocked, llk*^{rw468} (Wada et al., 2005)) were maintained according to standard procedures as described in Solnica-Krezel et al., 1994. Naturally spawned embryos were raised at 28-32°C, and staged by morphology (Kimmel et al., 1995). *Tg(vangl2:GFP-Vangl2)* fish were a gift from Anand Chandrasekhar (Columbia, MO, USA) (Sittaramane et al., 2013). MZ*tri*^{vu67} fish were obtained by germ cell transplantation described in Ciruna et al., 2002.

Whole-mount immunostaining

Embryos at shield stage (6hpf) to 5s stage (11.7hpf) were fixed in Prefer Fixative (Anatech) at room temperature for 30-50 minutes and rinsed in 1X PBS. Dechorionated embryos were incubated in permeabilization solution (0.5%TritonX-100, 5% Bovine Serum Albumin (BSA), 5%serum, 2%DMSO, 1X PBS) for 20 to 30 minutes. Then, embryos were incubated for 1 hour in blocking solution (0.1%Triton-100, 5%BSA, 10%serum, 2%DMSO, 1X PBS). Primary and secondary antibodies were diluted in the blocking solution. Embryos were incubated in primary antibody solution overnight and in secondary antibody solution one hour at room temperature. Embryos were rinsed and stored in 1X PBS at 4˚C. Primary antibodies dilutions: rabbit polyclonal anti-zebrafish Vangl2 (made against a C-terminal peptide for LSK lab) 1:500; anti-β-Catenin 1:250 (Sigma C7207); anti-RFP (Allele

Biotechnology, Cat # ACT-CM-MRRFP10) 1:500. Secondary antibodies dilutions: goat-anti-rabbit Alexa-488, (Invitrogen-Molecular Probes, Cat # A11034) 1:500; goat-anti-Rabbit Alexa-647 (Invitrogen-Molecular Probes, Cat # A21245) 1:500; goat-anti-mouse Alexa-568 (Invitrogen-Molecular Probes, Cat # A11031) 1:500; goat-anti-rat Alexa-568 (Invitrogen-Molecular Probes, Cat # A11077) 1:500.

Microscope image acquisition

For Nomarski time-lapse acquisition, live dechorionated embryos were mounted in 0.5% low melting point agarose (LMP, SeePlaque Agarose, Cambrex Bio Science Rockland, Inc; Cat#: 50100) in 0.3x Danieau's buffer, in wells in a 1.5% agarose block on MatTek glass-bottom petri dishes (Car#: P35G-1.0-14-C), f. For live imaging, embryos were kept at 28.5˚C with a heating chamber. For time-lapse, Z-stacks were collected with 30 sec or 1 min intervals using 40X (N.A, 0.75) objective.

Images were acquired using inverted Zeiss confocal microscope/LSM510 or Olympus inverted microscope/Quorum spinning disc confocal/Metamorph.

Quantification of cell shape and cell alignment

Cell shape (LWR) and cell alignment (angle) was performed using the Fiji software. Cell membrane boundaries were drawn manually. The quantification of the major and minor axis of the cell (fitting ellipse function) and angle was estimated by the software. LWR is defined as major axis/minor axis.

Synthetic RNA synthesis and Injections

RNA was synthesized using the mMESSAGE mMACHINE Ambion kit for SP6 (Cat# AM1340) or T7 (Cat# AM1354) promoter. RNA concentrations were measured on Nanodrop and electrophoresis gel. Injections were performed at 1- or 64-cell stage. 40pg or 200pg *Xdd1* synthetic mRNA was injected in one cell at 64-cell stage or at 1-cell stage, respectively. *Xenopus noggin* synthetic mRNA (100pg) achieved a strong dorsalization phenotype (Hammerschmidt et al., 1996)

Transplantation experiments

For homochronic/heterochronic transplantations donor embryos were injected with 100pg *mCherry* synthetic mRNA at 1-cell stage. For heterochronic transplantations donors and host embryos were fertized 2h apart. “Younger to Older” transplantation was performed by moving cells from sphere stage (4hpf) donor embryos into shield stage (6hpf) host embryos.

"Older to Younger" transplantation was performed in the reverse order. Embryos developed at 28.5˚C until the host embryos reached 80% epiboly (8.4hpf) and were fixed 40 minutes in Prefer fixative at room temperature. Homochronic control transplantations were performed at sphere stage and embryos were fixed at 80% epiboly. Whole mount immunostaining was performed in individual tubes for each set of host-donor embryos. The image acquisition settings were identical for each embryo in the individual sets.

Acknowledgements

We thank Margot Williams, Ryan Gray, Gina Castelvecchi and other members of the Solnica-Krezel lab for discussion and comments on the manuscript; and the Washington University School of Medicine in St Louis Zebrafish Facility Staff for excellent animal care. This work was supported in part by GM55101 grant to LSK from the National Institutes of Health, and the NICHD T32 HD049305 (Kelle H. Moley, Principal Investigator) to IR.

Author Contributions statement:

All authors conceived and designed the experiments, analyzed and discussed the data, and discussed the manuscript. I.R., and J.R.J., performed the experiments. D.S.S., A.C and L.S.-K. contributed reagents, materials and analysis tools I.R., wrote the manuscript with the assistance of L.S.-K., and J.R.J.

Figures

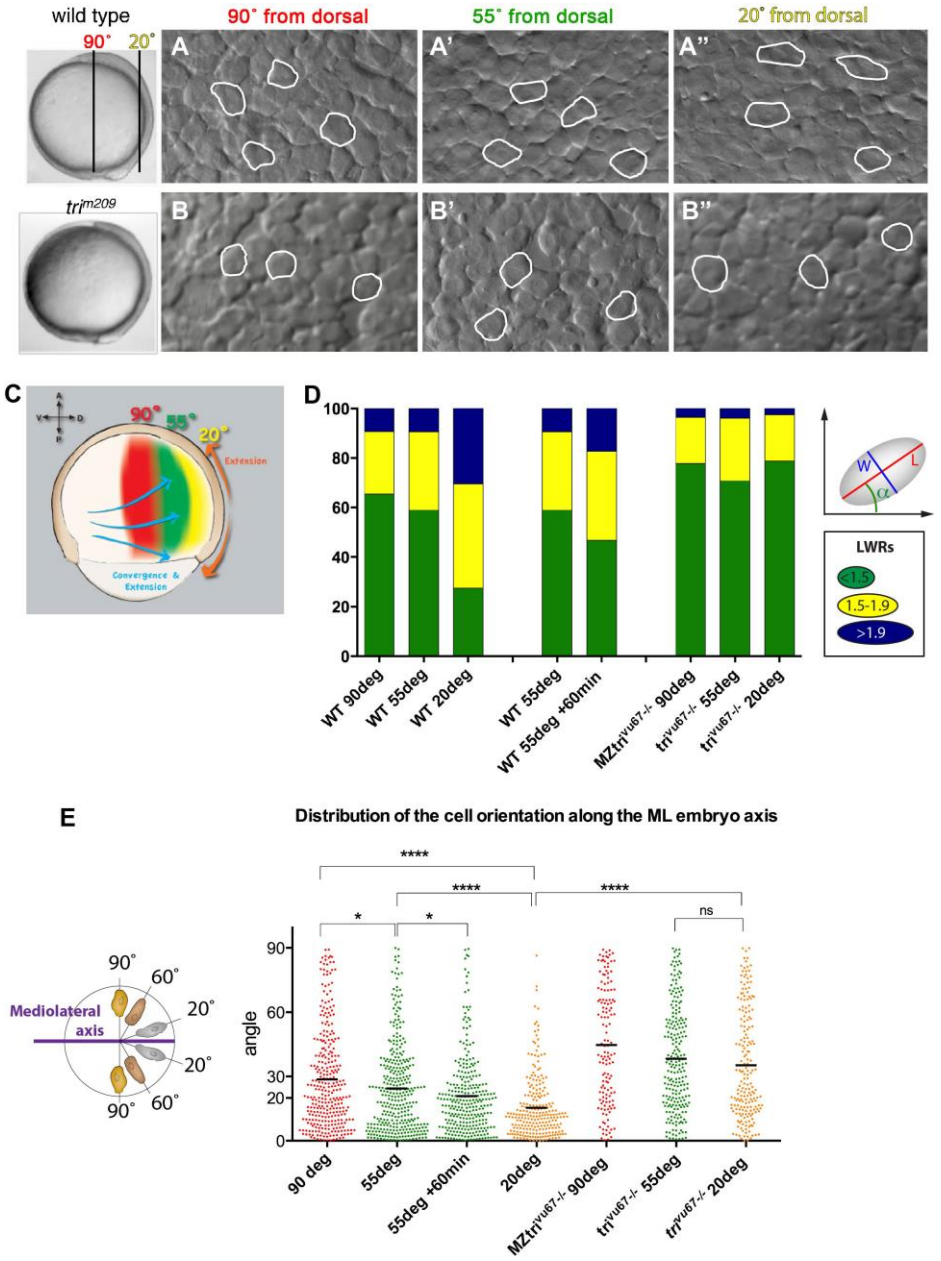

Fig1. **Spatiotemporal dynamics of mesodermal cells during C&E.**

(A-B") Nomarski images of mesodermal cells at various locations (90˚-A,B, 55˚-A',B', and 20˚ from dorsal –A",B") in the WT (A-A") and *tri*$^{vu67/vu67}$ (B-B") embryos at YPC stage (9.5 hpf). (C) Schematic representation of zebrafish embryo at 75%epiboly stage, showing the examined locations: 90˚ (red), 55˚ (green) and 20˚ (yellow). (D) Histogram representing the change in LWR of cells at examined locations in WT embryos, *tri*$^{vu67/vu67}$ *and MZtri*$^{vu67/vu67}$. *S*chematic representation explaining method used to measure the cell shape (LWR) and orientation (angle α). (E) Orientation of the major axis of each cell analyzed within examined locations at 9hpf in WT, *tri* $^{vu67/vu67}$ and *MZtri*$^{vu67/vu67}$ embryos, and at 9hpf and 10hpf at the 55˚ location. $^{*}P$<0.05, ****P<0.0001.

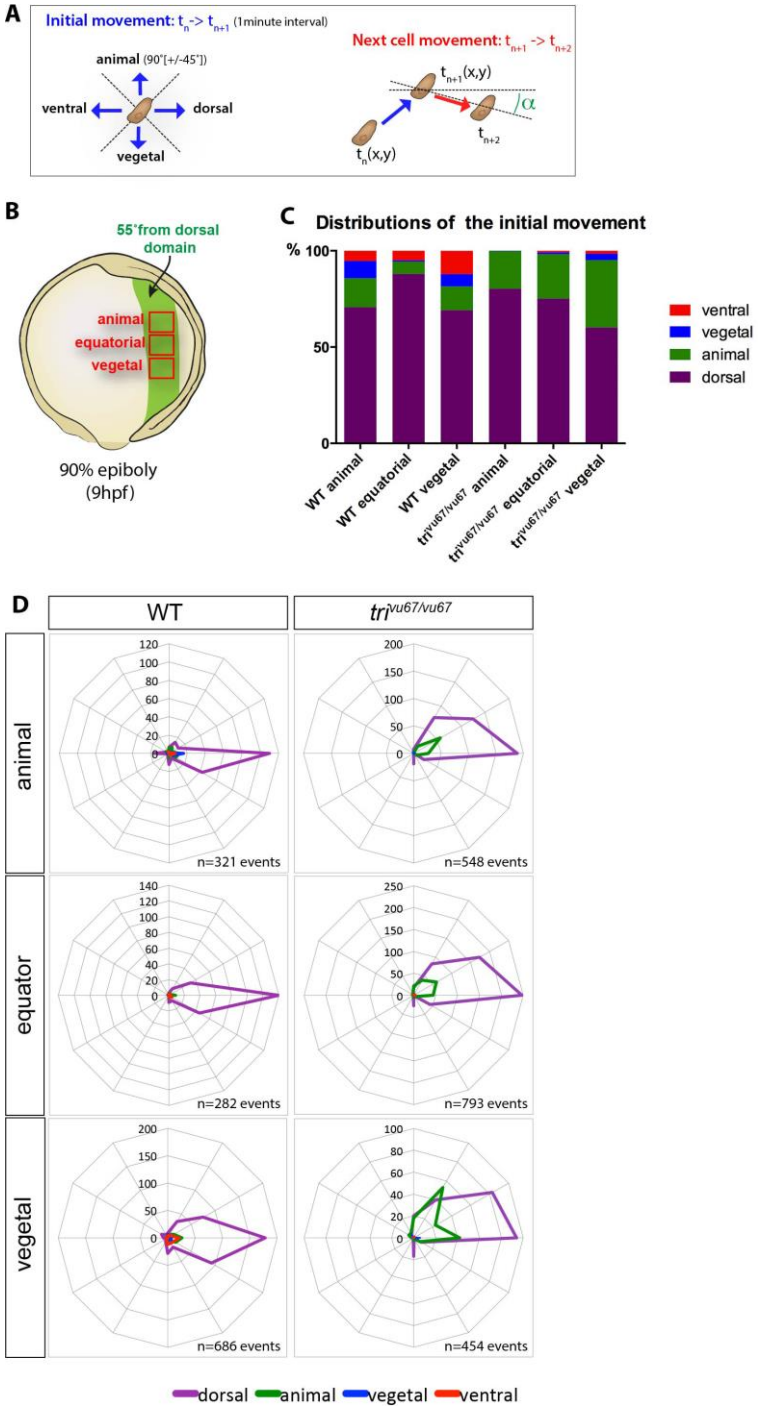

Fig2. **Cell behaviors at different positions along the anterior-posterior embryonic axis.**
(A) Schematic representation of the definition of the ***initial*** cell movement and ***next*** cell movement. (B) Drawing of a late gastrula embryo showing animal, equatorial and vegetal locations examined. (C) Distribution of the directionality of all cell movements during the time-lapse (60 minutes, 1-minute interval) in WT and *tri*$^{vu67/vu67}$ embryos in anterior, equatorial and posterior embryo locations. (D) Diagrams showing the orientation of the ***next*** cell movement pooled in categories referring to previous/***initial*** cell movement. On diagrams, animal is to the top, dorsal to the right, vegetal to the bottom and ventral to the left. Scale represents number of movement events.

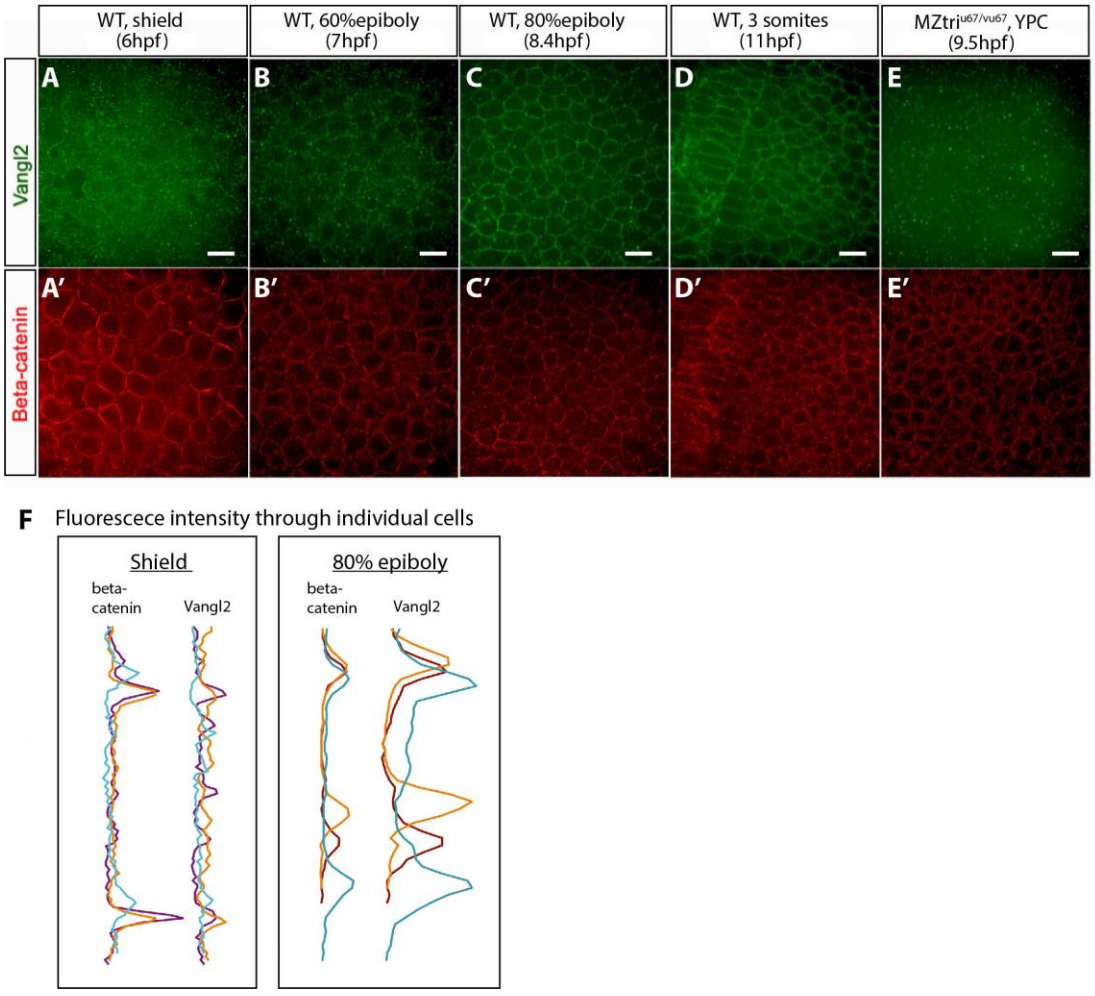

Fig3. **Dynamic Vangl2 intracellular localization during gastrulation.**

(A-E') Confocal images of WT embryos showing the intracellular and membrane localization of Vangl2 (A-E) and β-catenin (A'-E'). (F) Schematic representation of quantification of Vangl2 and β-catenin fluorescence intensity in individual cells (3 independent cells shown in lines of different color) at 6hpf and 8.4hpf, obtained using Fiji-plot profile tool through the length of the cell. Peaks correspond to cell membrane. Scale bars, 20 μm

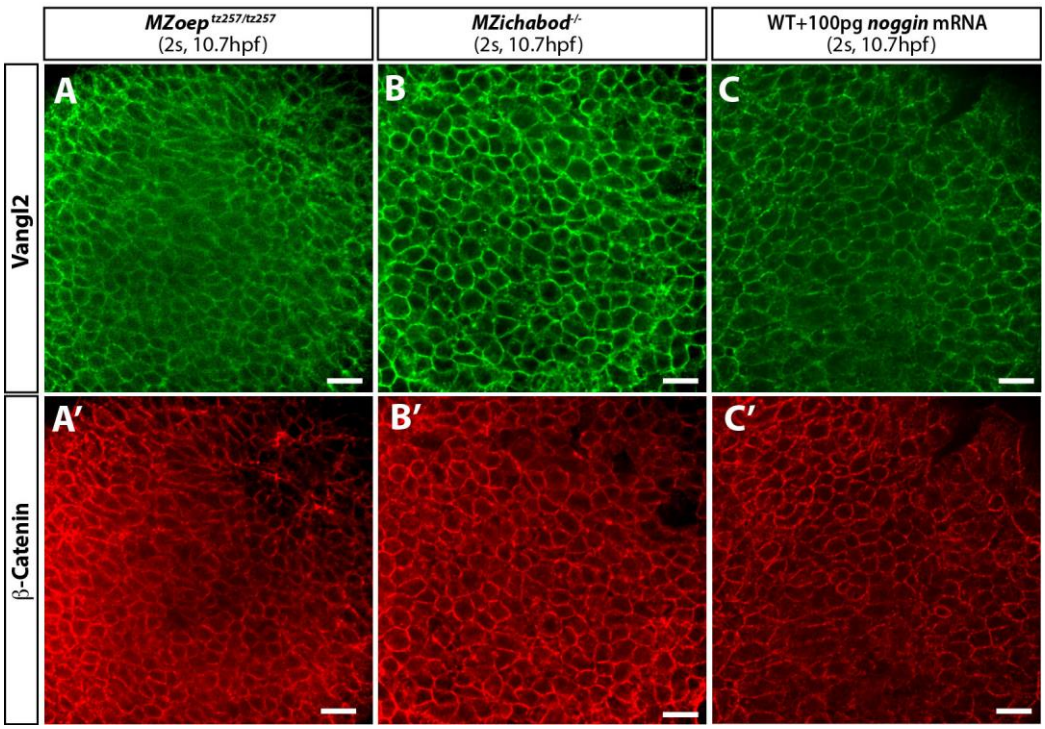

Fig4. **Membrane localization of Vangl2 in embryos with patterning defects**

Confocal images of whole mount immunostaining with antibodies against zebrafish Vangl2 C-terminus and β-catenin in *MZoep*$^{tz257/tz257}$ (A-A') and *MZichabod* (B-B') mutant embryos, and WT embryos injected with100pg *noggin* synthetic mRNA (C-C'). Scale bars, 20 μm

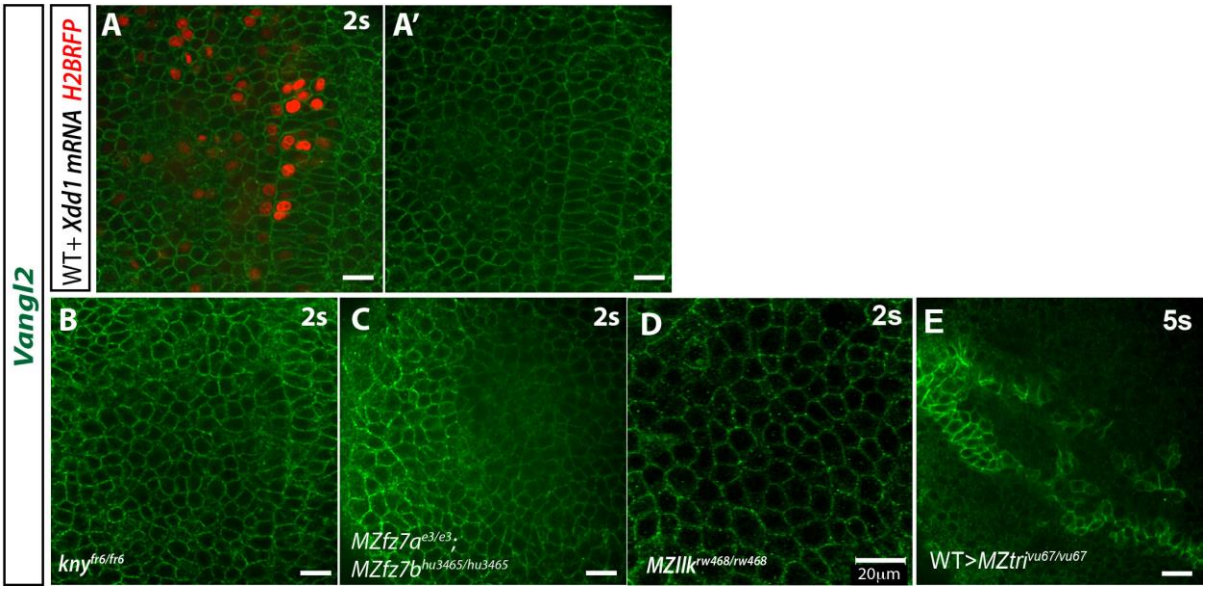

Fig5. **Tri/Vangl2 membrane localization in PCP mutant backgrounds**

Confocal images of whole mount immunostaining with antibody against zebrafish Vangl2 C-terminus in 2s stage (10.7hpf) embryos mosaically expressing Xdd1 and H2B-RFP (A-A'); in *kny*$^{fr6/fr6}$ (B); MZ*fz7*$^{ae3/e3}$;MZ*fz7b*$^{hu3465/hu3465}$ (C), MZ*llk*$^{rw468/rw468}$ (D); and *MZtri*$^{vu67/vu67}$ embryos (11.7hpf) containing transplanted WT cells (showing strong Vangl2 membrane expression) (E). Scale bars, 20 µm

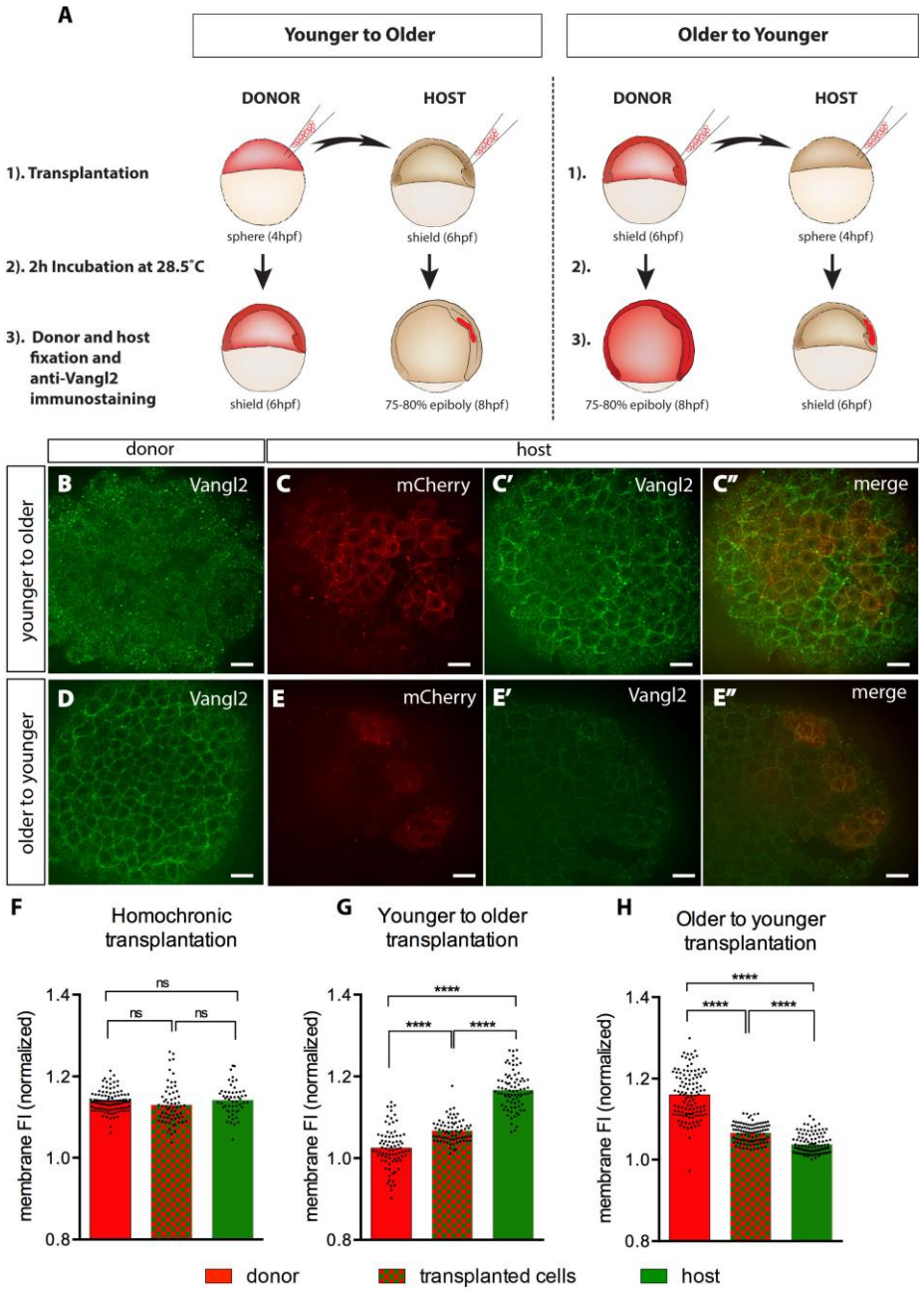

Fig6. **Heterochronic cell transplantations**

(A) Schematic representation of the experimental method. (B-E") Confocal images of donor and host embryos after immunostaining for Vangl2 and mCherry. (B-C") Results of transplantation from younger donor embryos into older hosts. (B) Donor embryo 2h post transplantation-6hpf, (C-C") Host embryo 2h post transplantation-8hpf. (D-E") Results of transplantation from older donor embryos into younger hosts. (D) Donor embryo 2h post transplantation-8hpf. (E-E") Host embryo 2h post transplantation-6hpf. (C,E) mCherry staining shows the transplanted cells. (F-H) Quantitative data showing the membrane fluorescence intensity in transplanted cells, and endogenous cells in host and donor embryos. (F,G,H) Quantitative data from homochronic (control) and heterochronic cell transplantations. ****P<0.0001. Scale bars, 20 μm.

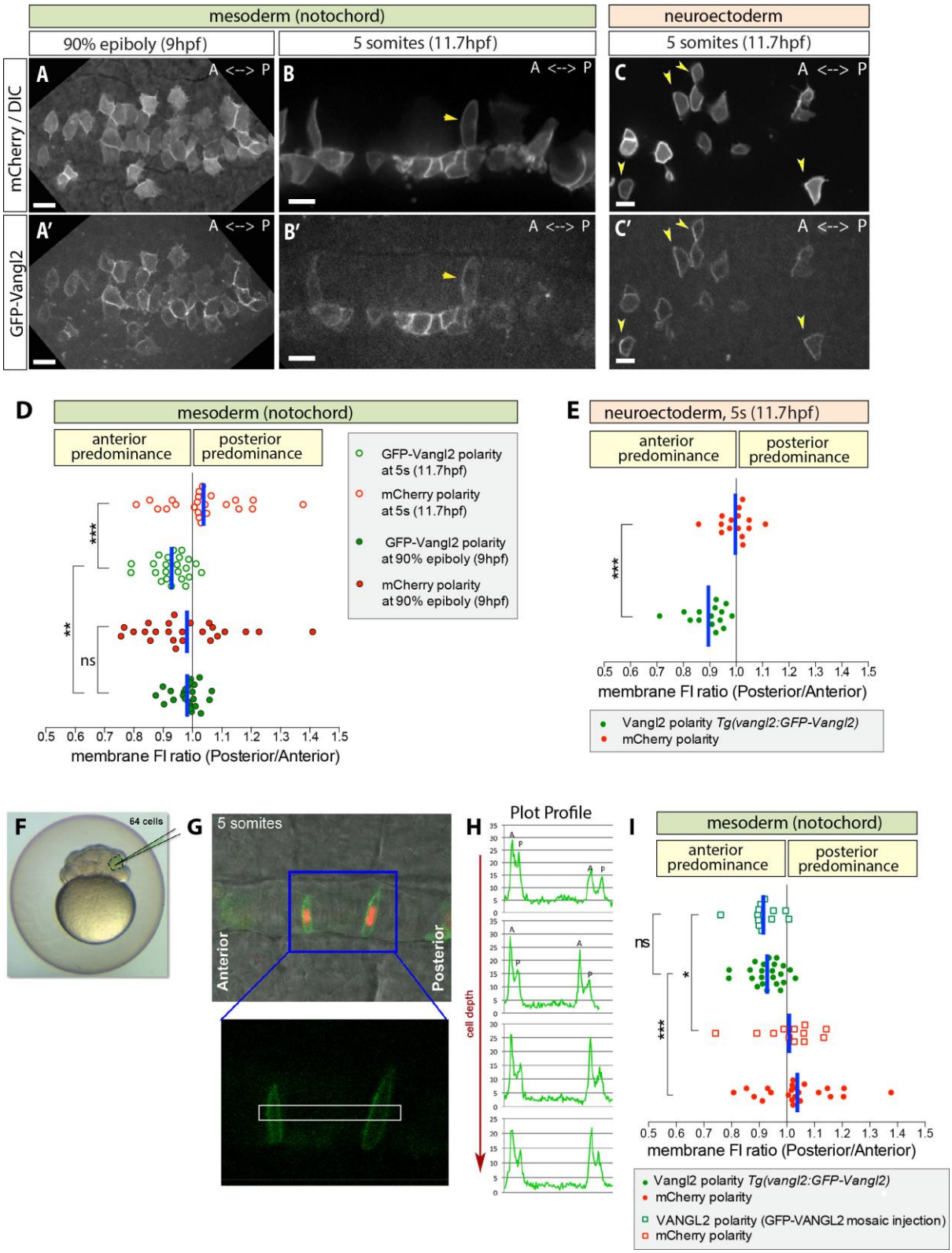

Fig7. **Enrichment of Tri/Vangl2 at anterior membranes of ML elongated cells.**

(A-C') Images of live embryos at 90% epiboly stage (9hpf) (A,A') or 5s stage (11.7pf) (B-C'). mCherry and GFP-Vangl2 expressing cells were transplanted from *Tg(vangl2:GFP-*

Vangl2) embryos into the WT unlabeled host. (D, E) GFP-Vangl2 and mCherry Posterior/Anterior membrane FI ratios of individual cells in the notochord at 90%epiboly stage (9hpf) and at 5-6s stage (11.7-12hpf) (D) or in the neuroectoderm at 5-6s stage (11.7-12hpf) (E). The blue bars represent the average of Posterior/Anterior FI ratios for each condition. (F-I) Vangl2 asymmetry analysis using the GFP-VANGL2 mosaic expression. (F) Modified picture of 64-cell stage embryo showing the mosaic synthetic mRNA injection performed. (G) Images of live embryos mosaically expressing GFP-VANGL2/H2B-RFP in notochord cells. White rectangle showing the area quantified with Fiji/plot profile. (H) Fiji/plot profile quantification of FI of 2 cells from (G) at 4 different z planes (confocal optical slices). (I) Comparison of GFP-VANGL2, GFP-Vangl2 and corresponding mCherry membrane FI ratios of analyzed individual cells in the notochord at 5-6s (11.7-12hpf) stage. $^{*}P<0.05$, $^{**}P<0.01$, $^{***}P<0.001$. Scale bars, 20 μm (A-A'), 10 μm (B-C').

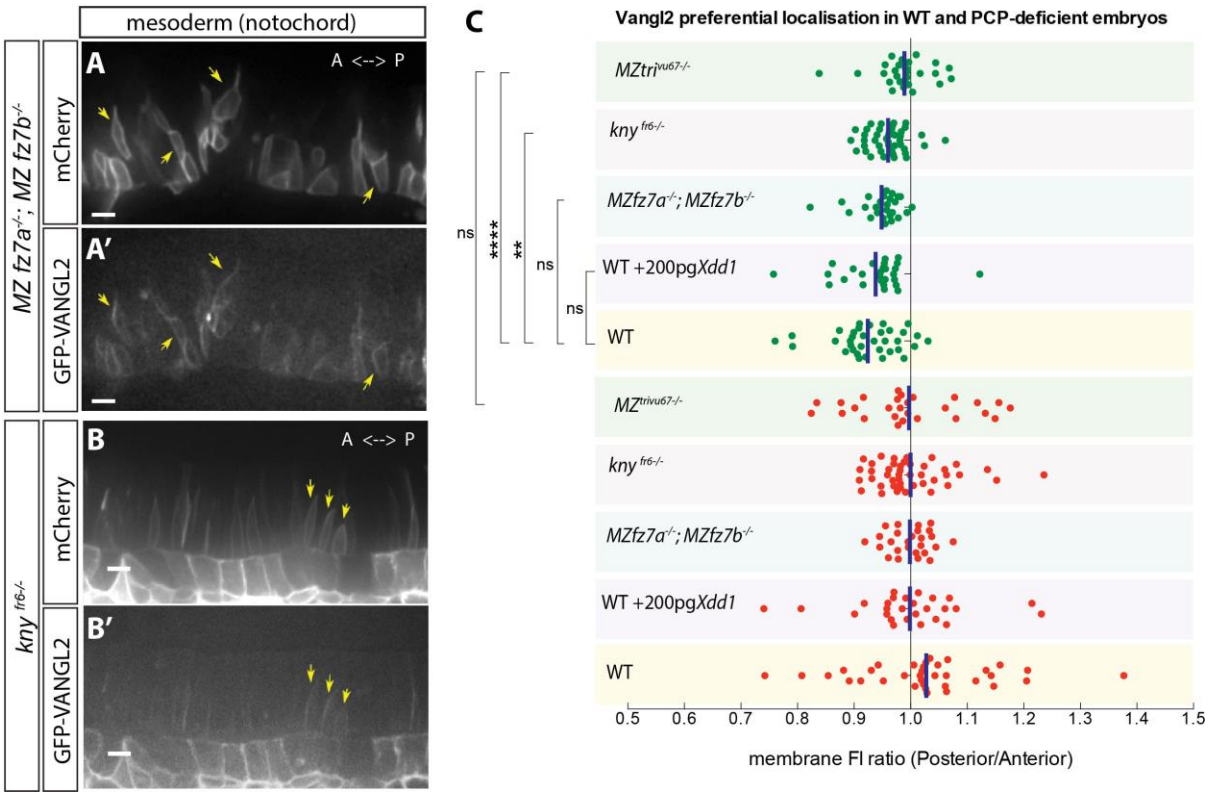

Fig8. **Vangl2 membrane localization in embryos with defective PCP signaling.**

(A-B') Images of live embryos mosaically expressing GFP-VANGL2 and mCherry. Yellow arrows are pointing out the individual cells showing anteriorly biased Vangl2 membrane localization. Scale bars, 10 μm.

(C) Quantification of mGFP (green) and mCherry (red) Posterior/Anterior membrane FI ratios obtained by analyzing individual cells in the notochord of 5-6 somite stage (11.7-12hpf) embryos in specified mutants or *Xdd1* RNA injected embryos. The data plot shows the quantification of either GFP-Vangl2 from *Tg(vangl2:GFP-Vangl2)* cells in *MZtri*$^{vu67-/-}$ and *Xdd1* injected embryos; or GFP-VANGL2 in *MZfz7a*$^{-/-}$;*MZfz7b*$^{-/-}$ and *kny*$^{fr6-/-}$ embryos. GFP-Vangl2 and GFP-VANGL2 quantification data are combined for the WT embryos. A blue bar represents the average of P/A FI ratios for each condition. $^{**}P<0.01$, $^{****}P<0.0001$.

References:

Adler, P. N. (2002). Planar signaling and morphogenesis in Drosophila. *Dev Cell* **2**, 525-535.

Adler, P. N., Krasnow, R. E. and Liu, J. (1997). Tissue polarity points from cells that have higher Frizzled levels towards cells that have lower Frizzled levels. *Curr Biol* **7**, 940-949.

Adler, P. N., Taylor, J. and Charlton, J. (2000). The domineering non-autonomy of frizzled and van gogh clones in the drosophila wing is a consequence of a disruption in local signaling [In Process Citation]. *Mech Dev* **96**, 197-207.

Amonlirdviman, K., Khare, N. A., Tree, D. R., Chen, W. S., Axelrod, J. D. and Tomlin, C. J. (2005). Mathematical modeling of planar cell polarity to understand domineering nonautonomy. *Science* **307**, 423-426.

Axelrod, J. D. (2001). Unipolar membrane association of Dishevelled mediates Frizzled planar cell polarity signaling. *Genes Dev* **15**, 1182-1187.

Bastock, R., Strutt, H. and Strutt, D. (2003). Strabismus is asymmetrically localised and binds to Prickle and Dishevelled during Drosophila planar polarity patterning. *Development* **130**, 3007-3014.

Bauer, H., Meier, A., Hild, M., Stachel, S., Economides, A., Hazelett, D., Harland, R. M. and Hammerschmidt, M. (1998). Follistatin and noggin are excluded from the zebrafish organizer. *Developmental biology* **204**, 488-507.

Borovina, A., Superina, S., Voskas, D. and Ciruna, B. (2010). Vangl2 directs the posterior tilting and asymmetric localization of motile primary cilia. *Nat Cell Biol* **12**, 407-412.

Bradley, E. W. and Drissi, M. H. (2011). Wnt5b regulates mesenchymal cell aggregation and chondrocyte differentiation through the planar cell polarity pathway. *Journal of cellular physiology* **226**, 1683-1693.

Chae, J., Kim, M. J., Goo, J. H., Collier, S., Gubb, D., Charlton, J., Adler, P. N. and Park, W. J. (1999). The Drosophila tissue polarity gene starry night encodes a member of the protocadherin family. *Development* **126**, 5421-5429.

Ciruna, B., Jenny, A., Lee, D., Mlodzik, M. and Schier, A. F. (2006). Planar cell polarity signalling couples cell division and morphogenesis during neurulation. *Nature* **439**, 220-224.

Coyle, R. C., Latimer, A. and Jessen, J. R. (2008). Membrane-type 1 matrix metalloproteinase regulates cell migration during zebrafish gastrulation: evidence for an interaction with non-canonical Wnt signaling. *Exp Cell Res* **314**, 2150-2162.

Das, G., Reynolds-Kenneally, J. and Mlodzik, M. (2002). The atypical cadherin Flamingo links Frizzled and Notch signaling in planar polarity establishment in the Drosophila eye. *Dev Cell* **2**, 655-666.

Devenport, D. and Fuchs, E. (2008). Planar polarization in embryonic epidermis orchestrates global asymmetric morphogenesis of hair follicles. *Nat Cell Biol* **10**, 1257-1268.

Dohn, M. R., Mundell, N. A., Sawyer, L. M., Dunlap, J. A. and Jessen, J. R. (2013). Planar cell polarity proteins differentially regulate extracellular matrix organization and assembly during zebrafish gastrulation. *Dev Biol* **383**, 39-51.

Dumortier, J. G., Martin, S., Meyer, D., Rosa, F. M. and David, N. B. (2012). Collective mesendoderm migration relies on an intrinsic directionality signal transmitted through cell contacts. *Proc Natl Acad Sci U S A* **109**, 16945-16950.

Furthauer, M., Thisse, B. and Thisse, C. (1999). Three different noggin genes antagonize the activity of bone morphogenetic proteins in the zebrafish embryo. *Developmental biology* **214**, 181-196.

Gao, B., Song, H., Bishop, K., Elliot, G., Garrett, L., English, M. A., Andre, P., Robinson, J., Sood, R., Minami, Y., et al. (2011). Wnt signaling gradients establish planar cell polarity by inducing Vangl2 phosphorylation through Ror2. *Dev Cell* **20**, 163-176.

Gray, R. S., Roszko, I. and Solnica-Krezel, L. (2011). Planar cell polarity: coordinating morphogenetic cell behaviors with embryonic polarity. *Dev Cell* **21**, 120-133.

Gritsman, K., Zhang, J., Cheng, S., Heckscher, E., Talbot, W. S. and Schier, A. F. (1999). The EGF-CFC protein one-eyed pinhead is essential for Nodal signaling. *Cell* **97**, 121-132.

Gubb, D., Green, C., Huen, D., Coulson, D., Johnson, G., Tree, D., Collier, S. and Roote, J. (1999). The balance between isoforms of the prickle LIM domain protein is critical for planar polarity in Drosophila imaginal discs. *Genes Dev* **13**, 2315-2327.

Hammerschmidt, M., Serbedzija, G. N. and McMahon, A. P. (1996). Genetic analysis of dorsoventral pattern formation in the zebrafish: requirement of a BMP-like ventralizing activity and its dorsal repressor. *Genes & development* **10**, 2452-2461.

Heisenberg, C. P., Tada, M., Rauch, G. J., Saude, L., Concha, M. L., Geisler, R., Stemple, D. L., Smith, J. C. and Wilson, S. W. (2000). Silberblick/Wnt11 mediates convergent extension movements during zebrafish gastrulation. *Nature* **405**, 76-81.

Jessen, J. R. and Solnica-Krezel, L. (2004). Identification and developmental expression pattern of van gogh-like 1, a second zebrafish strabismus homologue. *Gene Expr Patterns* **4**, 339-344.

Jessen, J. R., Topczewski, J., Bingham, S., Sepich, D. S., Marlow, F., Chandrasekhar, A. and Solnica-Krezel, L. (2002). Zebrafish trilobite identifies new roles for Strabismus in gastrulation and neuronal movements. *Nat Cell Biol* **4**, 610-615.

Keller, R., Davidson, L., Edlund, A., Elul, T., Ezin, M., Shook, D. and Skoglund, P. (2000). Mechanisms of convergence and extension by cell intercalation. *Philos Trans R Soc Lond B Biol Sci* **355**, 897-922.

Kilian, B., Mansukoski, H., Barbosa, F. C., Ulrich, F., Tada, M. and Heisenberg, C. P. (2003). The role of Ppt/Wnt5 in regulating cell shape and movement during zebrafish gastrulation. *Mech Dev* **120**, 467-476.

Kuss, P., Kraft, K., Stumm, J., Ibrahim, D., Vallecillo-Garcia, P., Mundlos, S. and Stricker, S. (2014). Regulation of cell polarity in the cartilage growth plate and perichondrium of metacarpal elements by HOXD13 and WNT5A. *Dev Biol* **385**, 83-93.

Lawrence, P. A., Casal, J. and Struhl, G. (2004). Cell interactions and planar polarity in the abdominal epidermis of Drosophila. *Development* **131**, 4651-4664.

Le Grand, F., Jones, A. E., Seale, V., Scime, A. and Rudnicki, M. A. (2009). Wnt7a activates the planar cell polarity pathway to drive the symmetric expansion of satellite stem cells. *Cell stem cell* **4**, 535-547.

Li, S., Esterberg, R., Lachance, V., Ren, D., Radde-Gallwitz, K., Chi, F., Parent, J. L., Fritz, A. and Chen, P. (2011). Rack1 is required for Vangl2 membrane localization and planar cell polarity signaling while attenuating canonical Wnt activity. *Proc Natl Acad Sci U S A* **108**, 2264-2269.

Li, X., Roszko, I., Sepich, D. S., Ni, M., Hamm, H. E., Marlow, F. L. and Solnica-Krezel, L. (2013). Gpr125 modulates Dishevelled distribution and planar cell polarity signaling. *Development* **140**, 3028-3039.

Lin, F., Sepich, D. S., Chen, S., Topczewski, J., Yin, C., Solnica-Krezel, L. and Hamm, H. (2005). Essential roles of G{alpha}12/13 signaling in distinct cell behaviors driving zebrafish convergence and extension gastrulation movements. *J Cell Biol* **169**, 777-787.

Ma, D., Yang, C. H., McNeill, H., Simon, M. A. and Axelrod, J. D. (2003). Fidelity in planar cell polarity signalling. *Nature* **421**, 543-547.

Mahaffey, J. P., Grego-Bessa, J., Liem, K. F., Jr. and Anderson, K. V. (2013). Cofilin and Vangl2 cooperate in the initiation of planar cell polarity in the mouse embryo. *Development* **140**, 1262-1271.

Marlow, F., Topczewski, J., Sepich, D. and Solnica-Krezel, L. (2002). Zebrafish Rho kinase 2 acts downstream of Wnt11 to mediate cell polarity and effective convergence and extension movements. *Curr Biol* **12**, 876-884.

Marlow, F., Zwartkruis, F., Malicki, J., Neuhauss, S. C., Abbas, L., Weaver, M., Driever, W. and Solnica-Krezel, L. (1998). Functional interactions of genes mediating convergent extension, knypek and trilobite, during the partitioning of the eye primordium in zebrafish. *Dev Biol* **203**, 382-399.

Merte, J., Jensen, D., Wright, K., Sarsfield, S., Wang, Y., Schekman, R. and Ginty, D. D. (2010). Sec24b selectively sorts Vangl2 to regulate planar cell polarity during neural tube closure. *Nat Cell Biol* **12**, 41-46; sup pp 41-48.

Montcouquiol, M., Sans, N., Huss, D., Kach, J., Dickman, J. D., Forge, A., Rachel, R. A., Copeland, N. G., Jenkins, N. A., Bogani, D., et al. (2006). Asymmetric localization of Vangl2 and Fz3 indicate novel mechanisms for planar cell polarity in mammals. *J Neurosci* **26**, 5265-5275.

Myers, D. C., Sepich, D. S. and Solnica-Krezel, L. (2002a). Bmp activity gradient regulates convergent extension during zebrafish gastrulation. *Dev Biol* **243**, 81-98.

---- (2002b). Convergence and extension in vertebrate gastrulae: cell movements according to or in search of identity? *Trends Genet* **18**, 447-455.

Nutt, S. L., Dingwell, K. S., Holt, C. E. and Amaya, E. (2001). Xenopus Sprouty2 inhibits FGF-mediated gastrulation movements but does not affect mesoderm induction and patterning. *Genes Dev* **15**, 1152-1166.

Panousopoulou, E., Tyson, R. A., Bretschneider, T. and Green, J. B. (2013). The distribution of Dishevelled in convergently extending mesoderm. *Dev Biol* **382**, 496-503.

Quesada-Hernandez, E., Caneparo, L., Schneider, S., Winkler, S., Liebling, M., Fraser, S. E. and Heisenberg, C. P. (2010). Stereotypical cell division orientation controls neural rod midline formation in zebrafish. *Curr Biol* **20**, 1966-1972.

Sepich, D. S., Calmelet, C., Kiskowski, M. and Solnica-Krezel, L. (2005). Initiation of convergence and extension movements of lateral mesoderm during zebrafish gastrulation. *Dev Dyn* **234**, 279-292.

Sepich, D. S., Myers, D. C., Short, R., Topczewski, J., Marlow, F. and Solnica-Krezel, L. (2000). Role of the zebrafish trilobite locus in gastrulation movements of convergence and extension. *Genesis* **27**, 159-173.

Sepich, D. S. and Solnica-Krezel, L. (2005). Analysis of cell movements in zebrafish embryos: morphometrics and measuring movement of labeled cell populations in vivo. *Methods Mol Biol* **294**, 211-233.

Shih, J. and Keller, R. (1992). Patterns of cell motility in the organizer and dorsal mesoderm of Xenopus laevis. *Development* **116**, 915-930.

Shimada, Y., Usui, T., Yanagawa, S., Takeichi, M. and Uemura, T. (2001). Asymmetric colocalization of Flamingo, a seven-pass transmembrane cadherin, and Dishevelled in planar cell polarization. *Curr Biol* **11**, 859-863.

Shindo, A. and Wallingford, J. B. (2014). PCP and septins compartmentalize cortical actomyosin to direct collective cell movement. *Science* **343**, 649-652.

Sittaramane, V., Pan, X., Glasco, D. M., Huang, P., Gurung, S., Bock, A., Li, S., Wang, H., Kawakami, K., Matise, M. P., et al. (2013). The PCP protein Vangl2 regulates migration of hindbrain motor neurons by acting in floor plate cells, and independently of cilia function. *Dev Biol* **382**, 400-412.

Sokol, S. Y. (1996). Analysis of Dishevelled signalling pathways during Xenopus development. *Current Biology* **6**, 1456 - 1467.

Solnica-Krezel, L. and Sepich, D. S. (2012). Gastrulation: making and shaping germ layers. *Annu Rev Cell Dev Biol* **28**, 687-717.

Strutt, D. I. (2001). Asymmetric localization of frizzled and the establishment of cell polarity in the Drosophila wing. *Mol Cell* **7**, 367-375.

---- (2002). The asymmetric subcellular localisation of components of the planar polarity pathway. *Semin Cell Dev Biol* **13**, 225-231.

Strutt, H. and Strutt, D. (2008). Differential stability of flamingo protein complexes underlies the establishment of planar polarity. *Current biology : CB* **18**, 1555-1564.

Strutt, H., Warrington, S. J. and Strutt, D. (2011). Dynamics of core planar polarity protein turnover and stable assembly into discrete membrane subdomains. *Dev Cell* **20**, 511-525.

Taylor, J., Abramova, N., Charlton, J. and Adler, P. N. (1998). Van Gogh: a new Drosophila tissue polarity gene. *Genetics* **150**, 199-210.

Theisen, H., Purcell, J., Bennett, M., Kansagara, D., Syed, A. and Marsh, J. L. (1994). dishevelled is required during wingless signaling to establish both cell polarity and cell identity. *Development* **120**, 347-360.

Tomlinson, A. and Struhl, G. (1999). Decoding vectorial information from a gradient: sequential roles of the receptors Frizzled and Notch in establishing planar polarity in the Drosophila eye. *Development* **126**, 5725-5738.

Topczewski, J., Sepich, D. S., Myers, D. C., Walker, C., Amores, A., Lele, Z., Hammerschmidt, M., Postlethwait, J. and Solnica-Krezel, L. (2001). The zebrafish glypican knypek controls cell polarity during gastrulation movements of convergent extension. *Dev Cell* **1**, 251-264.

Usui, T., Shima, Y., Shimada, Y., Hirano, S., Burgess, R. W., Schwarz, T. L., Takeichi, M. and Uemura, T. (1999). Flamingo, a seven-pass transmembrane cadherin, regulates planar cell polarity under the control of Frizzled. *Cell* **98**, 585-595.

Vinson, C. and Adler, P. N. (1987). Directional non-cell autonomy and the transmission of polarity information by the *frizzled* gene of *Drosophila*. *Nature* **329**, 549-551.

Wada, H., Iwasaki, M., Sato, T., Masai, I., Nishiwaki, Y., Tanaka, H., Sato, A., Nojima, Y. and Okamoto, H. (2005). Dual roles of zygotic and maternal Scribble1 in neural migration and convergent extension movements in zebrafish embryos. *Development* **132**, 2273-2285.

Wada, H. and Okamoto, H. (2009). Roles of noncanonical Wnt/PCP pathway genes in neuronal migration and neurulation in zebrafish. *Zebrafish* **6**, 3-8.

Wallingford, J. B., Fraser, S. E. and Harland, R. M. (2002). Convergent extension: the molecular control of polarized cell movement during embryonic development. *Dev Cell* **2**, 695-706.

Wallingford, J. B., Rowning, B. A., Vogeli, K. M., Rothbacher, U., Fraser, S. E. and Harland, R. M. (2000). Dishevelled controls cell polarity during Xenopus gastrulation. *Nature* **405**, 81-85.

Warga, R. M. and Kimmel, C. B. (1990). Cell movements during epiboly and gastrulation in zebrafish. *Development* **108**, 569-580.

Wolff, T. and Rubin, G. M. (1998). Strabismus, a novel gene that regulates tissue polarity and cell fate decisions in Drosophila. *Development* **125**, 1149-1159.

Wu, J., Roman, A. C., Carvajal-Gonzalez, J. M. and Mlodzik, M. (2013). Wg and Wnt4 provide long-range directional input to planar cell polarity orientation in Drosophila. *Nat Cell Biol* **15**, 1045-1055.

Yang, X., Dormann, D., Munsterberg, A. E. and Weijer, C. J. (2002). Cell movement patterns during gastrulation in the chick are controlled by positive and negative chemotaxis mediated by FGF4 and FGF8. *Dev Cell* **3**, 425-437.

Yin, C., Kiskowski, M., Pouille, P. A., Farge, E. and Solnica-Krezel, L. (2008). Cooperation of polarized cell intercalations drives convergence and extension of presomitic mesoderm during zebrafish gastrulation. *The Journal of cell biology* **180**, 221-232.

Zilber, Y., Babayeva, S., Seo, J. H., Liu, J. J., Mootin, S. and Torban, E. (2013). The PCP effector Fuzzy controls cilial assembly and signaling by recruiting Rab8 and Dishevelled to the primary cilium. *Mol Biol Cell* **24**, 555-565.

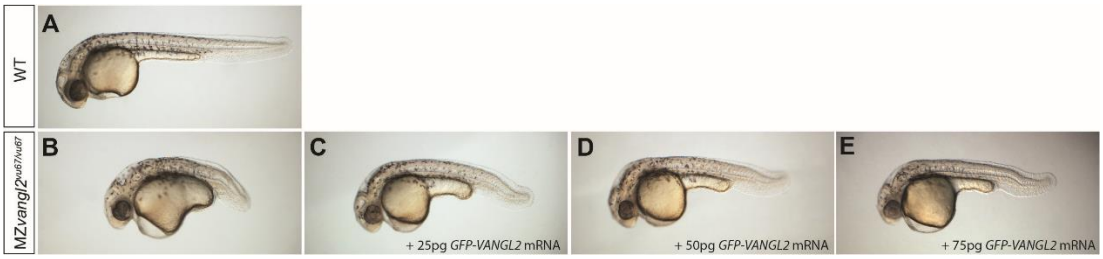

Fig. S1. Rescue of the MZ*vangl2*$^{vu67/vu67}$ phenotype with *GFP-VANGL2* synthetic mRNA. (A) 30hpf WT embryo. (B) 30hpf MZ*vangl2*$^{vu67/vu67}$ embryo. (C,D,E) 30hpf MZ*vangl2*$^{vu67/vu67}$ embryos injected at 1-cell stage with 25 pg, 50 pg or 75 pg synthetic *GFP-VANGL* mRNA.

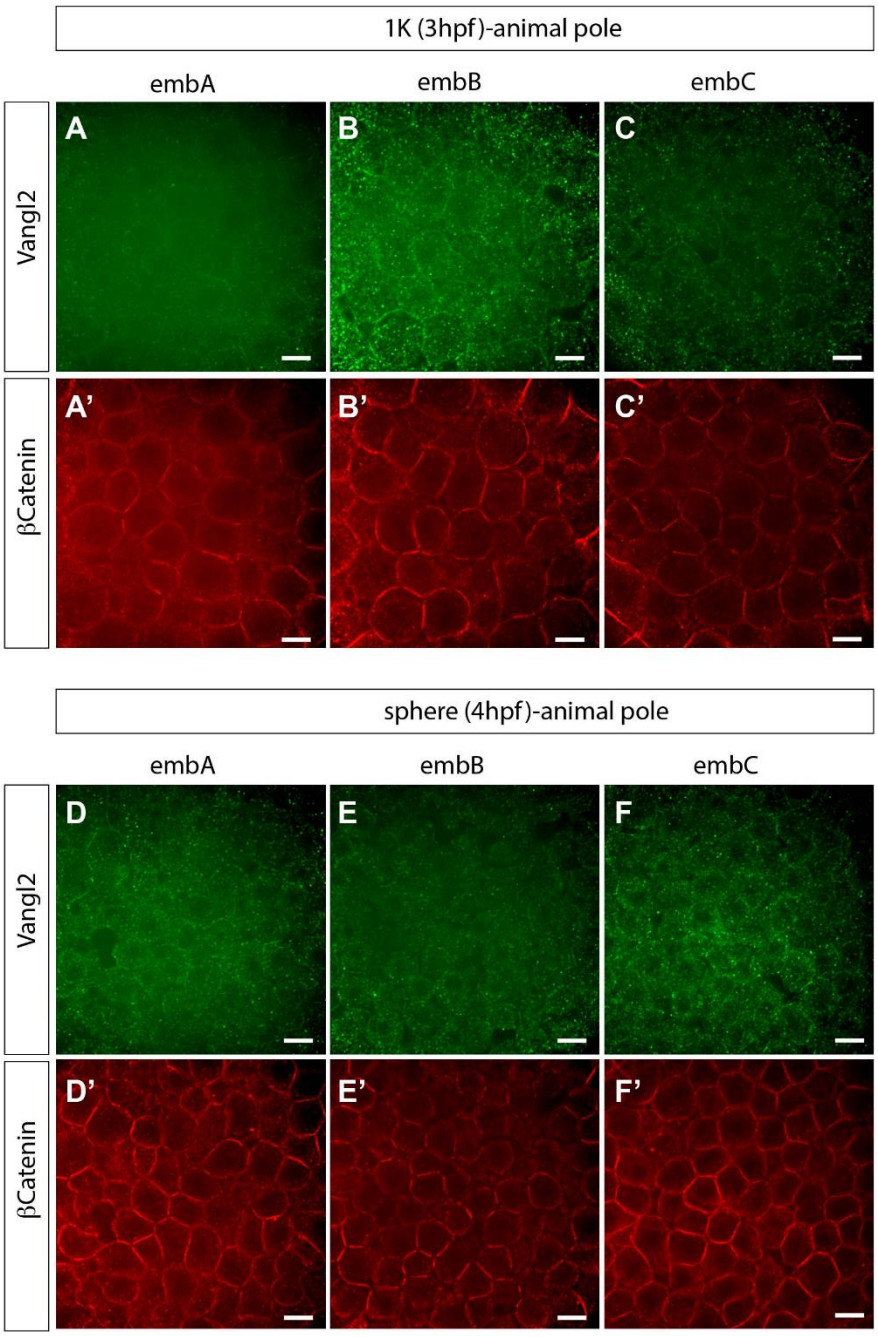

Fig. S2. Vangl2 protein expression at blastula stages.

Confocal images of embryos after immunostaining using the anti-C-terminal Vangl2 antibody (green) and anti-β-catenin (red). β-catenin staining was used as control in order to visualize the cell membranes. Several embryos are shown in order to represent the variability of the anti-Vangl2 staining at the membrane versus cytoplasm between embryos at the same developmental stage. All images were acquired at the animal pole location. (A-C') 3 different embryos at sphere stage (4hpf). (D-F') 3 different embryos at 1K stage (3hpf). Note the weak Vangl2 staining (green) at the membrane and the abundant puncta in the cytoplasm. Scale bars, 20 μm.

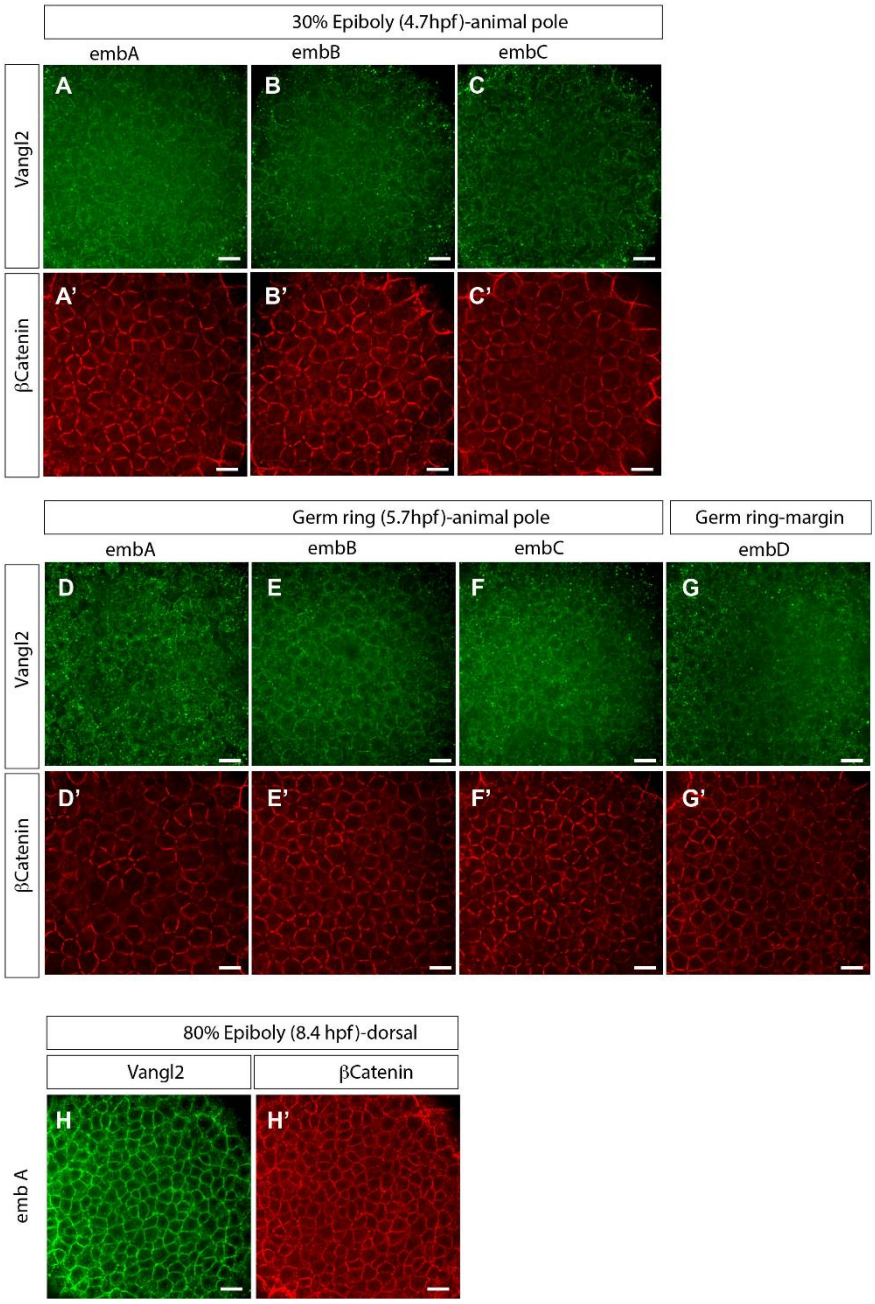

Fig S3. Vangl2 protein expression from 30% epiboly to 80% epiboly stages.

Confocal images of embryos after immunostaining using the anti-C-terminal zVangl2 antibody (green) and anti-βcatenin (red). β-catenin staining was used as control in order to visualize the cell membranes. Several embryos are shown in order to represent the slight variability of the anti-Vangl2 staining at the membrane versus cytoplasm between embryos at the same developmental stage. (A-C') 3 different embryos at 30% epiboly stage (4.7hpf). Images were acquired at the animal pole location. (D-F') 3 different embryos at germ ring stage (5.7hpf) (images acquired at the animal pole location). (G-G') embryos at germ ring stage (images acquired at the embryonic margin location). (H-H') embryos at 80% epiboly stage (8.4hpf) (images acquired at the dorsal location). Scale bars, 20 μm.

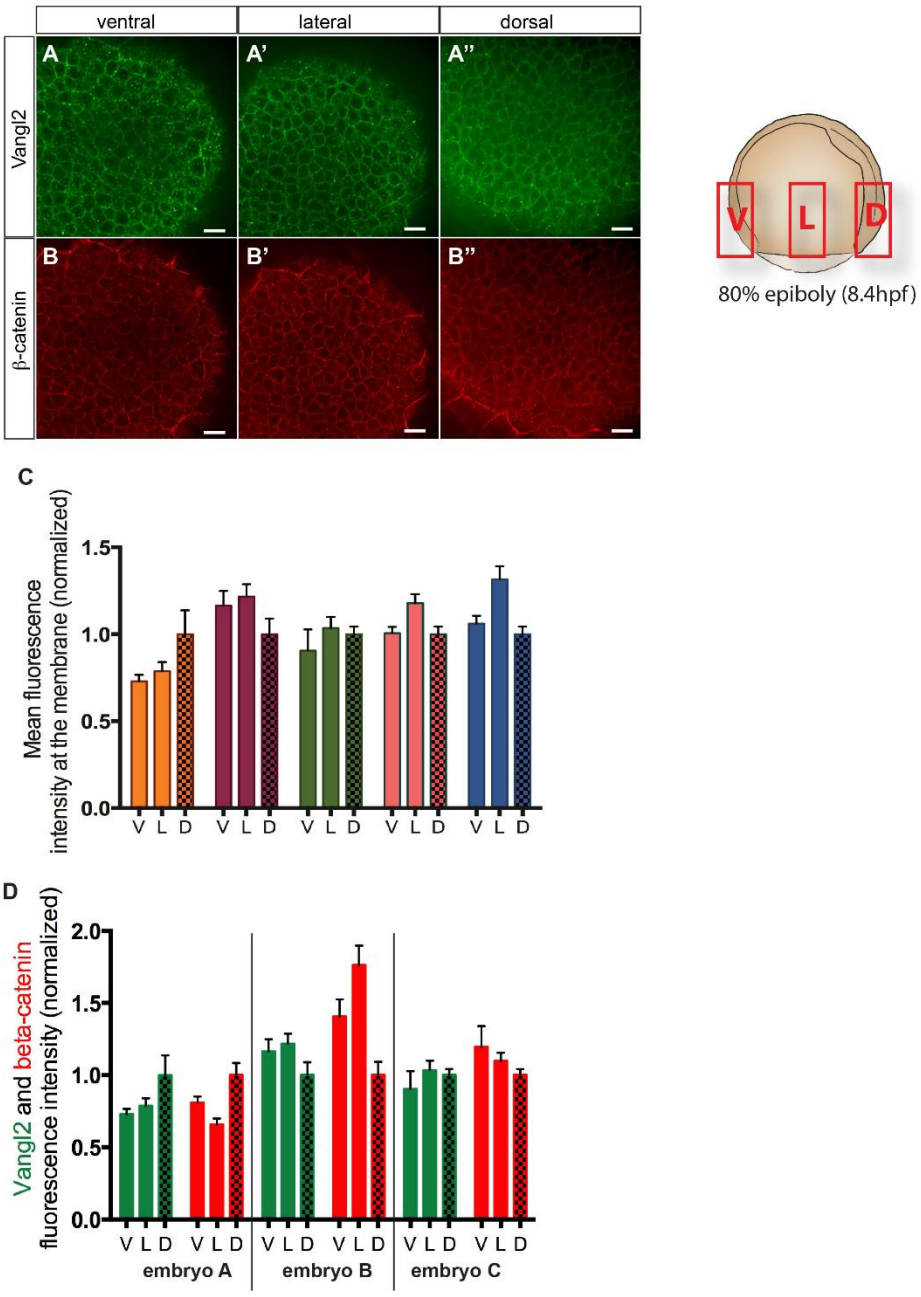

Fig S4. Vangl2 membrane localization in ventral, lateral or dorsal domain of the embryo does not show domain specific preference.

(A-B") Confocal images acquired in the ventral (A,B), lateral (A'B') and dorsal (A",B") domains in the embryo. Images were taken in all 3 domains of the same embryo and analyzed separately. Embryos at 80% epiboly stage (8.4hpf) were analyzed. (C) Quantitative data obtained from the analysis of the Vangl2 staining fluorescence intensity at the cell membrane in 5 different embryos (each embryo's D, V, L data set is in different color on the histogram). (D) Quantitative data comparing βcatenin (control) and Vangl2 staining for 3 different embryos in all D, L V domains, showing no domain specific preference for neither protein. All data were normalized such as dorsal=1. Scale bars, 20 μm.